UNIVERSIDAD DE
VALLADOLID
E.T.S.I DE
TELECOMUNICACIÓN

WARSAW UNIVERSITY OF
TECHNOLOGY
WEITI

MASTER´S THESIS

MASTER'S DEGREE IN TELECOMMUNICATIONS
ENGINEERING

Designing of Reconfigurable Intelligent Surfaces for 6G and mm-Wave

Author: Marcos Novoa González

Supervisor: Yevhen Yashchyshyn

Co-Supervisor: Eduardo Gómez Sánchez

March 10, 2025

TITLE:	Designing of Reconfigurable Intelligent Surfaces for 6G and mm-Wave
AUTHOR:	Marcos Novoa González
SUPERVISOR:	Yevhen Yashchyshyn
CO-SUPERVISOR:	Eduardo Gómez Sánchez

EXAMINING BOARD

CHAIRMAN:	Juan Carlos Aguado Manzano
SECRETARY:	Alfonso Bahillo Martínez
MEMBER:	Ramón de la Rosa Steinz
CHAIRMAN SUBSTITUTE:	María Jesús González Morales
SECRETARY SUBSTITUTE:	Julio Sánchez Curto
MEMBER SUBSTITUTE:	Juan Blas Prieto
DATE:	
GRADE:	

Abstract

The demand for ultra-fast data rates, low latency, and seamless connectivity is driving the development of 6G networks, which aim to overcome the limitations of 5G by leveraging higher frequency bands, including millimeter wave (mm-Wave) and terahertz (THz) spectra. However, these high-frequency bands present significant challenges, such as severe path loss and blockage sensitivity, which hinder reliable communication. Reconfigurable Intelligent Surfaces (RIS) have emerged as a promising solution to enhance signal propagation, spectral efficiency, and energy consumption by dynamically controlling electromagnetic waves.

This study explores the design and simulation of RIS for 6G and mm-Wave frequencies, focusing on a 2-bit tunable unit cell employing varactor diodes to achieve flexible beam reflection. Using CST Studio Suite, a detailed electromagnetic analysis is conducted, leading to the development of a 32×32 RIS array. Various linear coding schemes are implemented to evaluate their impact on beam steering and reflection angles. Simulation results demonstrate that the proposed RIS design effectively enhances signal strength and coverage, maintaining consistent performance across different incidence angles. The findings validate RIS as a key enabling technology for next-generation wireless communication systems, offering improved energy efficiency, spectral utilization, and connectivity.

KEYWORDS: 6G, RIS, Unit Cell, Varactor, Beam Steering, Metasurfaces, CST Studio Suite, Electromagnetic Simulation, Wireless Communication, Terahertz Communication.

Acknowledgments

Since no person or work exists in isolation, I want to express my deepest gratitude to all who have played a pivotal role in my journey. I am especially thankful to my dear parents, whose constant support, example, and dedication have been a beacon of inspiration in my life. The environment you've created, where work and love thrive, has been essential to my personal and academic growth. I also want to thank my brother, Diego, for his companionship, encouragement, and example, as well as my grandparents and the rest of my family for their unwavering love and support, which have provided a solid foundation in my path.

I am also grateful to God, who has shown me that working with love, honesty, and respecting His timing is a valuable path, and as long as I walk in the right direction, He will give me strength. As Philippians 4:13 says, "I can do all things through Christ who strengthens me." I also want to acknowledge myself for the moments of sacrifice and relentless effort during challenging times, always remembering that the road to success is rarely without obstacles.

One last mention to all the friendships I've made along the way. I especially want to highlight those from Colegio Maristas San Jose, where I've shared over 20 years of friendship that I'm sure will last forever, as well as those from the University of Valladolid and CMU Menendez Pelayo and from Balonmano Ademar Leon. A special shout-out to those from Student Depot in Warsaw, where I experienced Erasmus and who were the closest at the beginning of this project. In all these places, I found support and joy. Who I am is shaped by each of you.

I want to end by remembering to myself that it's crazy how much life improves when you do the right things. Do what you can, with

what you have, where you are. And in the end, try to leave the world a little more beautiful than you found it.

CONTENTS

“Dedicated to my parents, my brother Diego,
all my family and my friends.”

—

CHAPTER 1

INTRODUCTION

"Take the first step in faith.
You don't have to see the whole staircase,
just take the first step"

— Martin Luther King, *1963*.

1.1. Context and Motivation

The sixth generation of wireless communication (6G) aims to address the limitations of 5G by advancing connectivity, speed, and efficiency. As discussed in the Appendix A, 6G envisions a hyper-connected society, pushing the boundaries of communication technologies and extending coverage to air, sea, and space. This expansion is not only driven by the exponential growth in users but also by the increasing demands of emerging applications such as immersive virtual reality, telemedicine, and

autonomous systems. These applications require unprecedented bandwidth and network flexibility to function seamlessly.

Figure 1.1.: 6G Logo

To realize these ambitious goals, 6G leverages higher frequency bands, building upon the millimeter wave (mmWave) spectrum used in 5G. While mmWave has been instrumental in expanding 5G capabilities, 6G research is pushing toward even higher frequencies in the terahertz (THz) range. This progression into the THz spectrum is critical to achieve the massive data rates expected for 6G, with rates projected to reach up to 1 Tbps [19]. However, this advancement introduces significant challenges, such as signal propagation issues and sensitivity to physical obstructions.

Reconfigurable Intelligent Surfaces (RIS) have emerged as a promising solution to these challenges. RIS technologies enable new ways to manipulate the wireless environment, improving signal directionality and spectral efficiency, which is particularly valuable in high-frequency bands like mmWave and THz. These surfaces can potentially overcome the limitations associated with signal interference and physical obstacles, facilitating ultra-fast and reliable connectivity in complex, high-demand scenarios. Thus, optimizing RIS technologies for 6G networks becomes crucial in ensuring seamless communication in a hyper-connected world.

The technical groundwork for 6G is already underway, with major research initiatives focusing on advanced spectrum usage, intelligent networking, and the integration of AI-driven functions for real-time network optimization. International bodies such as the International Telecommunication Union (ITU) and the 3rd Generation Partnership Project (3GPP), as illustrated in Fig. 1.2, are working on developing standards and requirements under the designation IMT-2030, with the goal of deploying 6G networks by 2030 [5]. These technologies, including the mmWave and THz spectrum, visible light communication (VLC), and RIS, along with AI-based control mechanisms, are the

key enablers for realizing the vision of 6G and providing a highly efficient, adaptive, and resilient global communication network.

Figure 1.2.: Relationship between ITU and 3GPP

1.2. RIS: A Key to Future Networks

Reconfigurable Intelligent Surfaces (RIS) represent a transformative solution for 6G wireless networks, addressing both capacity and propagation challenges by reconfiguring the wireless environment. A RIS is a two-dimensional surface embedded with programmable elements that can control electromagnetic (EM) waves through phase shifts and amplitude modifications. Unlike traditional antenna arrays or active relays, RIS can operate passively, relying on external signals to achieve beamforming and signal redirection with minimal power consumption [10].

RIS plays a crucial role in the mm-Wave and terahertz (THz) bands, frequencies integral to 6G but highly susceptible to blockage and path loss. By reflecting signals in optimized directions, RIS can establish virtual line-of-sight (LoS) links even in environments where physical obstructions limit direct paths between users and base stations, as shown in Fig. 1.3. RIS improves spectral efficiency, compensating for the severe attenuation associated with high frequencies. They can be deployed on various surfaces, such as building facades, walls, and even vehicles, providing adaptable coverage and enhancing the connectivity of devices in challenging urban and indoor environments.

The growing interest in RIS technology is evident from the increasing number of published papers in recent years, each contributing new insights and innovations. For instance, reconfigurable transmitarrays have been extensively studied, such as a wideband 400-element electronically reconfigurable design for X-band applications

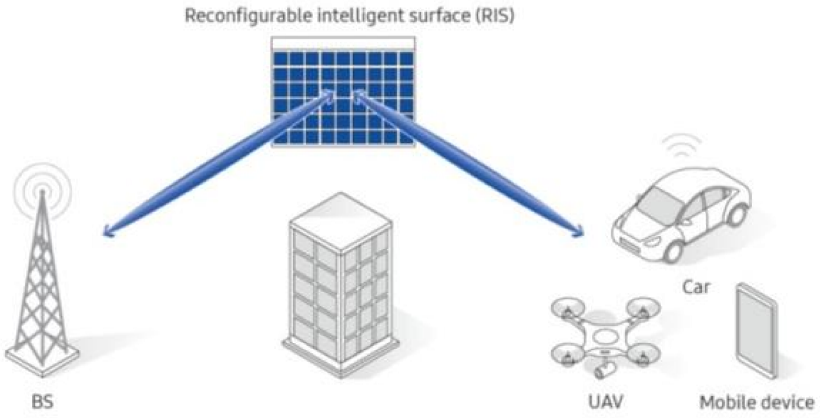

Figure 1.3.: Illustration of RIS improving signal redirection and enabling virtual line-of-sight in 6G networks.

[4] and a near-field coupled transmitarray for efficient 2D beam steering [12]. Further advancements include electronically steerable transmitarrays at Ka-band [23] and studies on UAV-mounted absorbing metasurfaces, exploring their mobility effects [20]. Additionally, research on software-defined metasurfaces integrated with machine learning techniques [18] and frequency reconfigurable polarization converters based on active metasurfaces [7] highlights the diversity of RIS applications. These studies reflect the broad potential of RIS, from enhancing beam steering capabilities to enabling intelligent wireless environments. The integration of RIS with other emerging 6G technologies, such as machine learning (ML) and intelligent network management, enables dynamic adaptation to changing user needs and environmental conditions. For instance, ML algorithms can optimize RIS configurations in real time to adjust to fluctuations in wireless channels or user mobility. This adaptability makes RIS a key enabler of smart, energy-efficient and high-capacity 6G networks.

Finally, commercial solutions, such as the XRifle Dynamic RIS for 5G coverage [17], demonstrate the real-world potential of RIS for enhancing signal propagation and coverage in both FR1 and FR2 frequency ranges, further showcasing RIS's promise in next-generation networks.

1.3. Objectives

The main objective of this thesis is to explore the potential of Reconfigurable Intelligent Surfaces (RIS) for next-generation wireless communication systems, particularly in

6G and mm-Wave applications and to implement a reflectarray with beam steering capability, leveraging these advancements to optimize wireless communication. To achieve this, the study is structured around the following specific objectives:

- **Introduction to RIS Technology:** Present the fundamental concepts of Reconfigurable Intelligent Surfaces, including their operating principles, key components, and relevance in modern wireless networks.
- **Understanding the Implementation Workflow:** Examine the standard design and implementation workflow for RIS systems, analyzing existing implementations to gain insight into their operation and performance.
- **Design and Development of a New RIS Implementation:** Propose a RIS unit cell and array configuration tailored for beam steering and beam redirection, ensuring practical feasibility and efficiency.
- **Electromagnetic Simulation:** Simulate the proposed RIS design using CST Studio Suite to evaluate its electromagnetic performance, including key parameters such as reflection coefficient (S11) and Radar Cross Section (RCS).
- **Analysis of Simulation Results:** Assess the effectiveness of the RIS designed by interpreting the simulation data.
- **Exploring Potential Applications and Practical Implementation:** Discuss the possible real-world applications of the designed RIS, highlighting its potential impact on wireless networks.

1.4. Methodology

To achieve the proposed objectives, the following methodology is followed:

1. **Literature Review:** Conduct an in-depth review of existing RIS technologies, including their theoretical foundations, implementation strategies, and applications in wireless networks.
2. **Conceptual Design:** Define the key parameters and structural configuration of the RIS, selecting the most suitable materials and components for efficient performance.

3. **Simulation and Modeling:** Implement the RIS design in CST Studio Suite, performing electromagnetic simulations to assess its behavior under various conditions.

4. **Analysis and Validation:** Evaluate simulation results by analyzing performance metrics such as reflection coefficients and beam steering capabilities.

5. **Conclusions and Future Work:** Summarize key findings, highlight the contributions of this study, and suggest possible future improvements or extensions of the work.

CHAPTER 2

THEORETICAL FUNDAMENTALS

"The whole world steps aside
for the man who knows where he is going."
— Antoine de Saint-Exupéry - The Little Prince, *1943*.

2.1. Terahertz communications

Terahertz (THz) communications are emerging as a crucial technology for 6G and future wireless networks, offering the potential to handle exponentially growing data demands with data rates reaching terabits per second. Operating in the THz band (0.1–10 THz), these frequencies provide vast, underutilized bandwidths that could alleviate spectrum scarcity and support data-intensive applications such as ultra-fast backhaul links [9] [25]. However, realizing THz communications in practical settings entails overcoming unique propagation challenges that differ from those encountered in sub-6 GHz and millimeter-wave (mmWave) bands.

2.1.1. Propagation Characteristics and Challenges

1. **High Path Loss:** In the THz band, signal propagation is highly susceptible to path loss. Free Space Path Loss (FSPL) is the inevitable attenuation experienced by a wave propagating in free space between two isotropic antennas. It is described by the Friis transmission formula given by:

$$P_r(d) = \frac{P_t \lambda^2}{(4\pi)^2 d^2} = \frac{P_t A_{\text{et}} A_{\text{er}}}{d^2 \lambda^2} \tag{2.1.1}$$

   where λ is the wavelength, d is the distance the wave will travel, P_t is the transmit power, and A_{et} and A_{er} represent the effective areas of the transmitting and receiving antennas, respectively. Based on Eq. 2.1.1, Fig. 2.1 shows the FSPL for a link for three different separation distances up to 3 THz.

   The severe path loss in THz bands often necessitates line-of-sight (LoS) connections, as even minor obstacles can significantly attenuate signals [9].

2. **Blockage Sensitivity:** Due to the extremely short wavelength of THz waves (in the millimeter to sub-millimeter range), THz signals are particularly sensitive to blockages. Physical objects, including small particles, can act as obstructions, effectively blocking or scattering the signal. This characteristic not only complicates indoor and urban deployment but also requires careful planning of antenna placement and beamforming strategies to ensure robust connectivity [25].

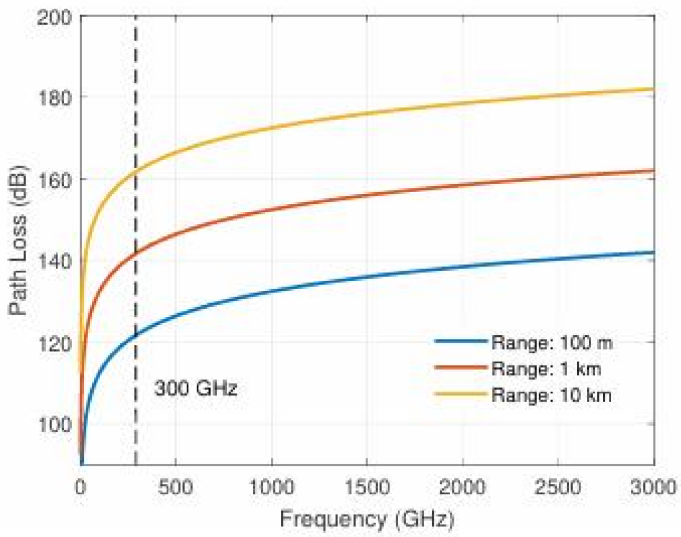

Figure 2.1.: Free space path loss for the frequency range 1-3,000 GHz with unity gain Tx and Rx antennas.

3. **Molecular Absorption:** Molecular absorption further limits the signal range in the THz band, as energy is absorbed by atmospheric molecules, particularly water vapor. This leads to frequency-dependent losses, creating distinctive "transmission windows" where signal attenuation is minimized and "absorption peaks" where attenuation is maximized, as shown in Fig 2.2.

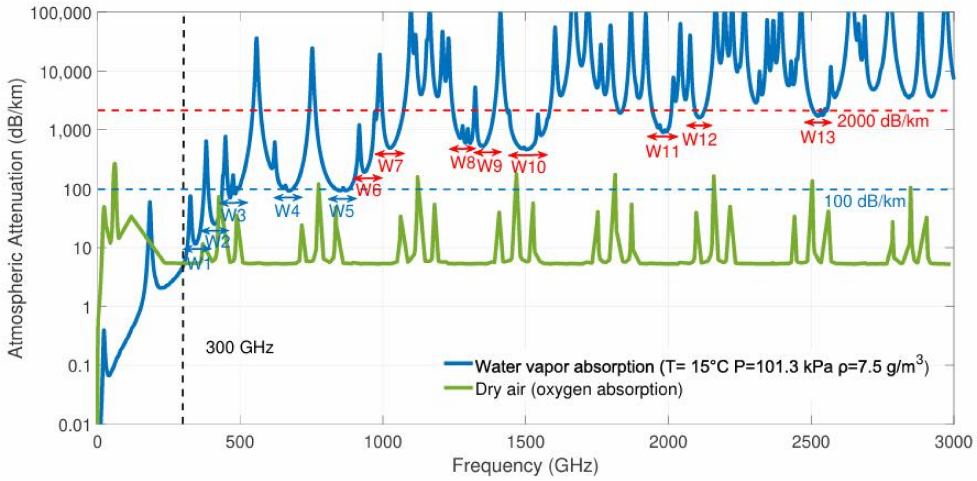

Figure 2.2.: Atmospheric attenuation in free space for the range 1-3,000 GHz.

4. **Channel Sparsity and Multipath Effects:** The propagation environment at THz frequencies is characterized by sparse multipath channels, where only a limited number of paths carry significant energy due to high reflection and scattering losses in non-line-of-sight (NLoS) conditions. This sparsity, combined with the strong directive nature of THz antennas, presents a challenge for traditional multiple-input multiple-output (MIMO) systems, which rely on multiple paths for spatial multiplexing gains. To address these issues, advanced channel modeling and antenna design, including ultra-massive MIMO (UM-MIMO), are required to maximize both data rates and coverage [9] [25].

2.1.2. Techniques for Overcoming Propagation Challenges

To mitigate these propagation challenges, several approaches are being explored in the THz communications field:

1. **Spectrum Management and Adaptive Transmission:** Adaptive spectrum management techniques that exploit "transmission windows" in the THz band allow for dynamic spectrum allocation based on environmental conditions. Distance-aware multi-carrier (DAMC) schemes, for example, use spectral regions within transmission windows for longer distances while avoiding high-absorption frequencies, optimizing bandwidth usage for multi-user scenarios. Additionally, techniques like temporal broadening of signals within absorption peaks can be leveraged for secure communications, as the rapid attenuation with distance can help limit eavesdropping range [25].

2. **Advanced Beamforming and Antenna Arrays:** Highly directional beamforming through hybrid beamforming architectures (HBAs) and ultra-massive MIMO arrays can help combat high path loss and focus THz energy along narrow paths, improving signal strength and reducing interference. Graphene-based nano-antennas, capable of supporting THz frequencies, offer promise for efficient, compact antenna arrays. These approaches provide robust connectivity and compensate for propagation losses [9].

3. **Multi-Connectivity and Reconfigurable Intelligent Surfaces (RIS):** Multi-connectivity (MC) strategies allow devices to simultaneously connect to multiple access points (APs), increasing reliability in environments prone to blockages. Reconfigurable intelligent surfaces (RIS), which dynamically adjust the phase of reflected signals,

can create virtual line-of-sight (LoS) paths, overcoming obstacles and extending coverage. Together, MC and RIS technologies aim to create resilient and flexible THz communication systems by compensating for the line-of-sight requirements and high sensitivity to blockages [25].

2.2. Reconfigurable Intelligent Surfaces

Reconfigurable Intelligent Surfaces (RIS) are emerging as a transformative technology in wireless communications, especially in the context of 6G networks. These surfaces manipulate electromagnetic (EM) waves to overcome propagation challenges and improve the efficiency of wireless systems. By dynamically altering the behavior of EM waves in terms of phase, amplitude, and polarization, RIS enables a more adaptive, intelligent, and energy-efficient wireless environment.

- **Metasurfaces:** At the heart of RIS are metasurfaces—engineered two-dimensional structures composed of subwavelength unit cells that interact with incident EM waves in a programmable manner. These metasurfaces serve as the physical platform for RIS functionality, enabling the redirection, focusing, and manipulation of EM waves without requiring active transmission. Each metasurface consists of an array of unit cells designed to exhibit unique electromagnetic properties, which collectively shape the wavefront in desired patterns.
- **Unit Cells:** Unit cells are the fundamental building blocks of RIS metasurfaces. They are subwavelength-sized elements that control the local response of the metasurface to incident EM waves. By tuning the unit cells, RIS can modify the wavefront in terms of:

  1. Phase: Controlling the phase of the reflected or transmitted wave enables precise beam steering or focusing.
  2. Amplitude: Adjusting the amplitude can enhance or suppress certain signals, aiding in interference management.
  3. Polarization: Changing the polarization of waves can optimize signal propagation for specific scenarios.

  The behavior of unit cells is often programmable, allowing RIS to dynamically adapt to changes in the wireless environment.

- **Electronic Components:** The programmability of RIS is achieved through electronic components embedded within or connected to the unit cells. These components enable real-time reconfiguration of the surface properties:

  1. Varactors: Voltage-controlled capacitors that alter the phase and amplitude of reflected waves [1].
  2. PIN Diodes: Semiconductor switches used to control the state of unit cells, enabling rapid reconfiguration of metasurface properties [8].
  3. Microelectromechanical Systems (MEMS): Miniature mechanical devices that provide high precision and energy efficiency for tuning unit cells [13].

  These components are selected based on application requirements such as speed, power consumption, and operational frequency range.

- **Control Systems:** To orchestrate the dynamic behavior of RIS, advanced control systems are employed:

  1. Microcontroller Units (MCUs): Lightweight processors responsible for basic control and management of RIS operations, particularly in static or low-complexity scenarios.
  2. Field-Programmable Gate Arrays (FPGAs): High-performance programmable hardware used for real-time, complex control of RIS in dynamic environments. FPGAs are particularly advantageous in handling the low-latency, high-throughput demands of 6G networks.

  These control systems interface with the electronic components of the unit cells, executing algorithms that optimize the RIS configuration based on network conditions, user locations, and channel characteristics.

- **Interaction with EM Waves:** RIS functionality is fundamentally based on the interaction between its metasurfaces and incident EM waves. By leveraging the programmability of unit cells, RIS can achieve:

  1. Beamforming: Directing signal energy toward specific users or regions, maximizing signal strength and reducing interference.
  2. Beam Steering: Dynamically redirecting signals to maintain connectivity with moving users or mitigate blockages.

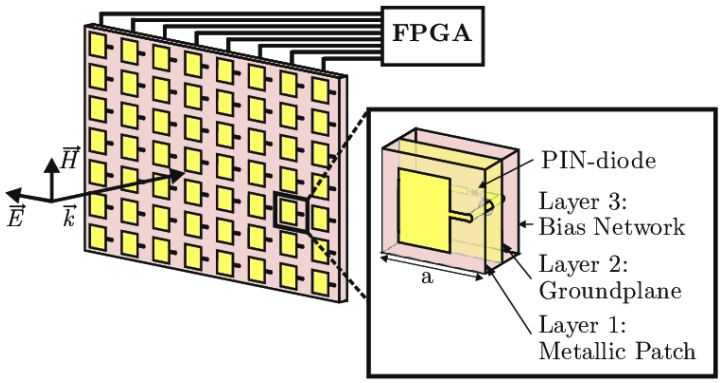

Figure 2.3.: Example of PIN-diode based Unit Cell and RIS Array Configuration controlled by FPGA

3. Polarization Control: Optimizing signal propagation by adjusting wave polarization, particularly in challenging environments.

4. Absorption Control: RIS can also manage absorption of electromagnetic waves. By configuring unit cells to dissipate energy instead of reflecting it, RIS can reduce unwanted signal propagation. This functionality is particularly useful for applications requiring enhanced security, such as UAV-mounted RIS systems, where controlled absorption minimizes signal leakage and interference [2].

These capabilities make RIS a powerful tool for enhancing coverage, spectral efficiency, and energy efficiency in 6G networks.

- **Integration with 6G Networks:** The integration of RIS into 6G networks represents a paradigm shift in wireless communication. RIS can be deployed on various surfaces, such as building facades, walls, and vehicles, transforming passive structures into active components of the communication infrastructure. This integration is further enhanced by the use of machine learning and intelligent network management systems, which optimize RIS configurations in real-time to adapt to environmental changes and user demands.

  By addressing key challenges in high-frequency bands like terahertz and millimeter waves, RIS is set to play a critical role in achieving the seamless, ultra-fast, and energy-efficient connectivity envisioned for 6G.

2.3. Beam Scanning and Beam steering

Beam scanning and beam steering are fundamental techniques in advanced wireless communication systems, particularly in the context of Reconfigurable Intelligent Surfaces (RIS) and 6G networks. These methods enhance signal coverage, improve link reliability, and increase data throughput by dynamically adjusting the direction and focus of transmitted or received beams.

2.3.1. Beam Scanning

Beam scanning involves systematically varying the beam's direction to cover a wide angular range. This technique is especially useful for:

- Rapidly searching for users or targets within a given area.
- Facilitating initial access procedures where the base station scans multiple directions to detect user equipment.
- Addressing scenarios with uncertain or dynamic channel conditions, where the optimal beam direction is not predetermined.

Figure 2.4 illustrates the concept of beam scanning by showing how the beam sweeps through different angles to cover a broad area.

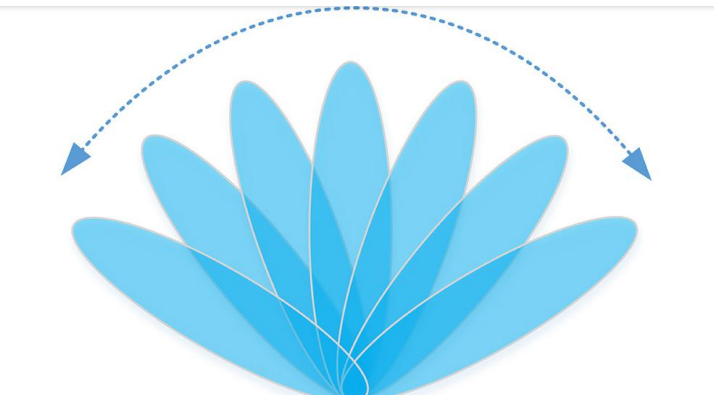

Figure 2.4.: Conceptual illustration of beam scanning in a wireless communication system.

2.3.2. Beam Steering

Beam steering, in contrast, refers to the dynamic adjustment of the beam direction to focus on a specific target or user. Unlike beam scanning, which covers a wide area, beam steering is used to maintain a strong, directed beam based on real-time channel conditions. Its key benefits include:

- Enhancing signal strength and reducing interference by focusing energy towards the intended user.
- Maintaining robust communication links in mobile environments by continuously adapting the beam direction as users move.
- Improving spectral efficiency by enabling spatial reuse of the spectrum.

Figure 2.5 shows a typical beam steering scenario, where an antenna array adjusts its phase distribution to direct the beam toward a target user.

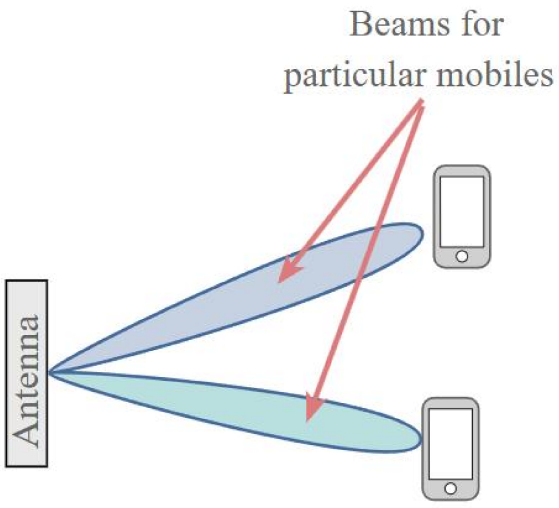

Figure 2.5.: Illustration of beam steering using an antenna array to focus the beam on a specific target.

Both techniques are critical in overcoming propagation challenges, especially at higher frequencies such as millimeter-wave and terahertz bands, where highly directional beams are necessary to combat severe path loss and interference. Their integration into RIS technology facilitates real-time adaptation of the wireless environment, significantly improving network performance.

2.4. Varactor

A varactor is a critical component in the reconfiguration of the RIS that is designed in the next chapters of this project. It is a voltage-controlled capacitor whose capacitance varies with the applied bias voltage. This property makes the varactor ideal for tuning the electromagnetic response of the RIS unit cells, enabling dynamic control over the phase and amplitude of the reflected signals. The operation principle of the varactor is based on the variation of the depletion region in a semiconductor junction under different bias voltages. As the bias voltage changes, the effective capacitance of the varactor changes accordingly. This variation allows the RIS to adjust the phase shift of the reflected wave [26].

Figure 2.6 shows a typical schematic of a varactor diode, illustrating its internal structure and Figure 2.7 shows the typical voltage-dependent capacitance variation. This fundamental behavior is exploited when the varactor is integrated into a RIS unit cell.

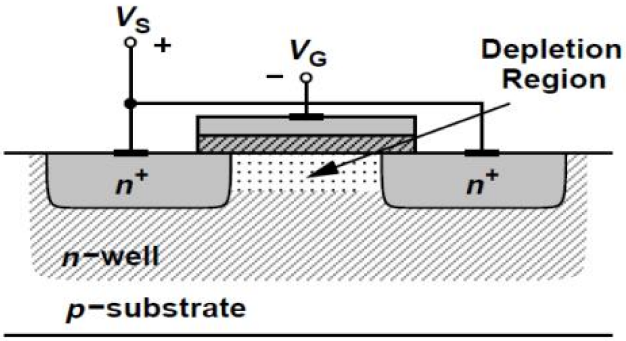

Figure 2.6.: Schematic diagram of a varactor diode illustrating its voltage-dependent capacitance.

The rapid reconfiguration capabilities provided by varactors are crucial for high-frequency applications, such as those anticipated in 6G networks, where efficient control over electromagnetic wave propagation is required to mitigate path loss and interference. Moreover, their low power consumption compared to other active components makes varactors a favorable choice for energy-efficient designs.

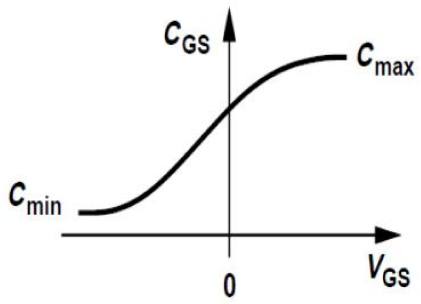

Figure 2.7.: Typical voltage-dependent capacitance variation of a varactor.

2.5. Performance Parameters: S_{11} and RCS

To evaluate the performance of the unit cell and the overall Reconfigurable Intelligent Surface (RIS), the main parameters that are going to be analyzed are the reflection coefficient (S_{11}) and the Radar Cross Section (RCS). These parameters provide critical information on the reflection behavior and scattering characteristics of the unit cell, which are essential for assessing its effectiveness in beam scanning and beam steering applications.

2.5.1. Reflection Coefficient (S_{11})

The reflection coefficient, denoted as S_{11}, represents the ratio of the reflected power to the incident power at the input port of the unit cell. It is expressed in terms of magnitude and phase, and it provides insight into:

- **Reflection Amplitude:** Indicates the amount of power reflected by the unit cell, influencing the efficiency of the RIS.
- **Phase Response:** Determines the phase shift introduced by the unit cell, which is critical for controlling the wavefront.

2.5.2. Radar Cross Section (RCS)

Radar Cross Section (RCS) is a measure of the scattering properties of an object when illuminated by an electromagnetic wave. For RIS applications, analyzing the RCS is essential to understand:

- **Scattering Pattern:** Indicates how the incident wave is scattered by the RIS.
- **Monostatic and Bistatic RCS:** These metrics provide information about the scattered power in the direction of the incident wave (monostatic) and in other directions (bistatic).

2.6. Floquet Boundaries

Floquet boundaries are essential in the analysis and design of periodic structures such as RIS unit cells. They impose periodic boundary conditions that simulate an infinite array, allowing for an accurate evaluation of the electromagnetic behavior of a single cell while accounting for its interactions with neighboring cells. This approach helps to determine:

- **Resonance Frequencies:** The periodic conditions influence the resonance frequencies of the unit cell.
- **Scattering Behavior:** The overall scattering parameters are affected, as the boundaries define the interaction between the incident wave and the periodic structure.

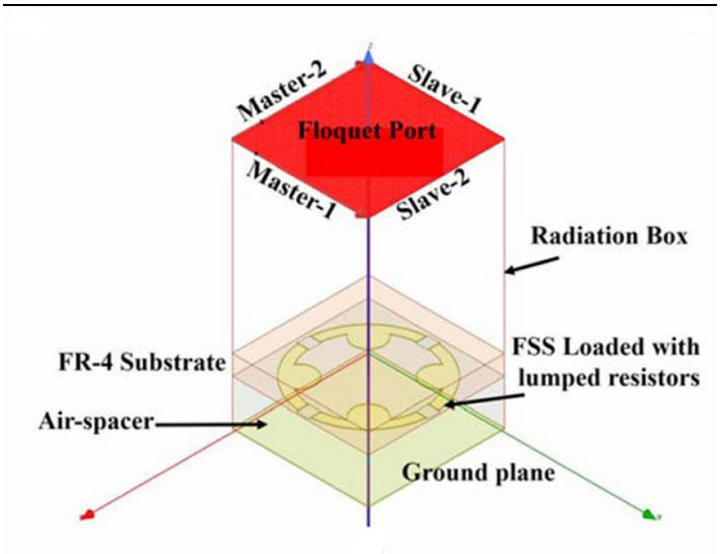

Figure 2.8.: Schematic illustration of Floquet boundaries applied to a unit cell. The periodic boundary conditions enable the simulation of an infinite array. From "A novel modified circular ring-based broadband polarization-insensitive angular stable circuit analog absorber (CAA) for RCS applications" [3]

CHAPTER 3

Designs and Practical Implementations of RIS

"Stay Hungry,
Stay Foolish."
— Steve Jobs, *2005*.

In this section, we will examine the operation of specific examples of Reconfigurable Intelligent Surface (RIS) antennas to better understand their functionality and application in modern wireless communication systems. Instead of discussing the general design principles, we will focus on how these particular RIS antennas work in practice, analyzing their key features, operational mechanisms, and how they contribute to enhancing communication performance. Through concrete examples, we aim to provide a detailed exploration of RIS technology in action, shedding light on its potential and real-world effectiveness.

3.1. Design and Analysis of a 1-Bit RIS Unit Cell with Mechanical Reconfiguration at 28 GHz

The first step in designing a reconfigurable intelligent surface (RIS) is the development of its unit cell, which defines the overall performance and capabilities of the RIS. One of the implementations described in the literature utilizes microelectromechanical systems (MEMS) technology for the mechanical reconfiguration of its unit cells. In particular, the study "Mechanical Design of a 1-Bit Reconfigurable Intelligent Surface Unit Cell" presents a mechanically tunable RIS unit cell operating at 28 GHz, achieving a binary phase modulation of 180° through controlled mechanical displacement [13].

The proposed unit cell consists of a metallic cylinder with a reconfigurable end element that can be moved along the z-axis inside a cylindrical cavity. This movement modifies the reflected wave's phase response, enabling two discrete phase states (1-bit), where the phase difference between them is approximately 180°.

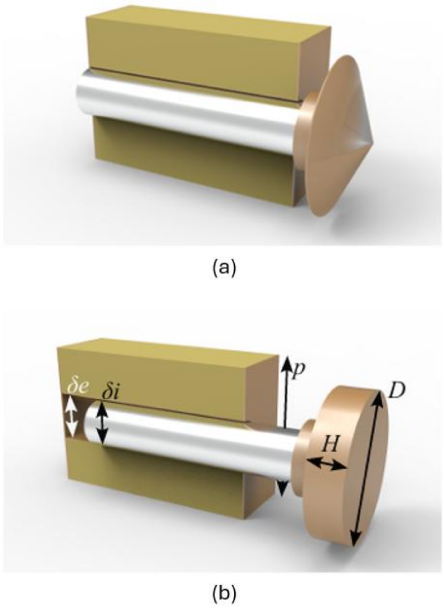

Figure 3.1.: Two implementations of the mechanically reconfigurable RIS unit cell: (a) Conical shape, (b) Cylindrical shape. Adapted from "Mechanical Design of a 1-Bit Reconfigurable Intelligent Surface Unit Cell." [13]

As shown in Figure 3.1, two different geometries for the reconfigurable element were analyzed: a conical and a cylindrical shape. The study found that the conical

shape provides superior electromagnetic performance, as it extends phase stability over a broad frequency range (25 to 31 GHz) and mitigates unwanted resonances [13].

To validate performance, simulations were conducted in CST Studio Suite, evaluating the reflection coefficient (S_{11}) for both designs. Figure 3.2 illustrates the reflection magnitude and phase shift between the two states of the unit cells, demonstrating the effectiveness of the conical shape in achieving stable phase variation.

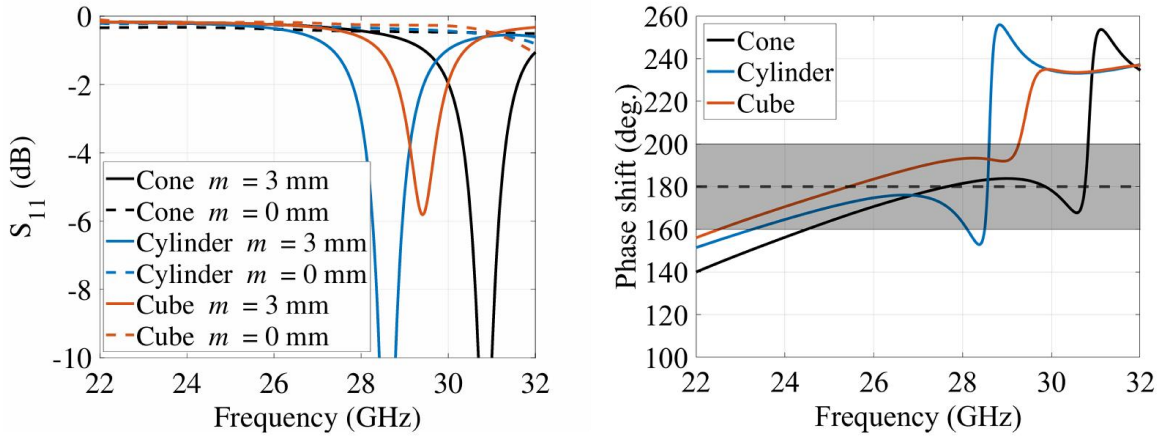

Figure 3.2.: Simulated reflection coefficient (S_{11}) of the mechanically reconfigurable RIS unit cells. (a) Magnitude, (b) Phase shift between states. From "Mechanical Design of a 1-Bit Reconfigurable Intelligent Surface Unit Cell." [13]

For prototyping, 3D printing with stereolithography (SLA) was used for the dielectric structure, followed by metallization using a conductive spray. A tolerance analysis demonstrated the robustness of the design against dimensional and conductivity variations. Despite deviations in the cone dimensions or the conductivity of the metallization, the unit cell maintains adequate performance within the target frequency band [13].

This implementation demonstrates that using MEMS for the mechanical reconfiguration of RIS is a viable alternative, offering good performance at millimeter-wave frequencies and accessible fabrication through 3D printing and metallization techniques.

3.2. A New 1 Bit Electronically Reconfigurable Transmitarray

Now that an example of the design of a unit cell has been discussed, we will examine another case from the literature where a new unit cell is used to develop a complete RIS for beam scanning that can be very useful for several systems, as was said in the chapter 2. In a recent study, a novel 1 bit electronically reconfigurable transmitarray that enables two-dimensional beam scanning with high gain and a low-profile design in the C-band (4-8 GHz) was proposed. Unlike traditional phased arrays that require complex phase-shifting networks, this design leverages a compact unit cell based on a Fabry–Pérot (F–P) resonant cavity and integrated PIN diodes for dynamic phase control [15].

The cornerstone of the transmitarray is its unit cell. As depicted in Figure 3.3, the unit cell consists of two layers of F4B substrates separated by an air gap. This unit cell uses two metallic layers with grating structures that form a Fabry–Pérot (F–P) resonant cavity. These gratings are placed on the top and bottom layers of the unit cell, oriented orthogonally to each other. The F–P cavity creates constructive and destructive interferences as the wave bounces between the two gratings. The middle layer contains a C-shaped structure with circular and two rectangular gaps, oriented at $\pm 45^\circ$ with respect to the y–axis. Two oppositely oriented PIN diodes (model SMP1340-040LF) are loaded across the gaps so that one diode is ON while the other is OFF—thus realizing a 180° phase shift between State 0 and State 1.

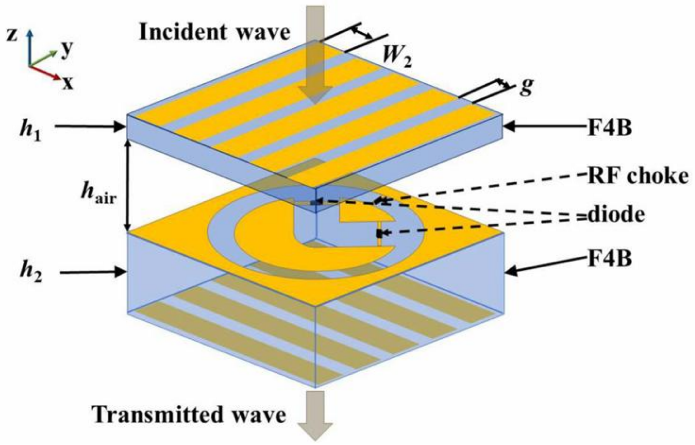

Figure 3.3.: Structure of the transmitarray unit cell. From "A New 1 Bit Electronically Reconfigurable Transmitarray" [15].

Simulations reveal that in the 4.7–5.3 GHz range, the transmission coefficient (S_{21}) remains high with nearly identical amplitude responses and a constant 180° phase difference between the two states. Figure 3.4 illustrates the simulated transmission amplitude and phase responses.

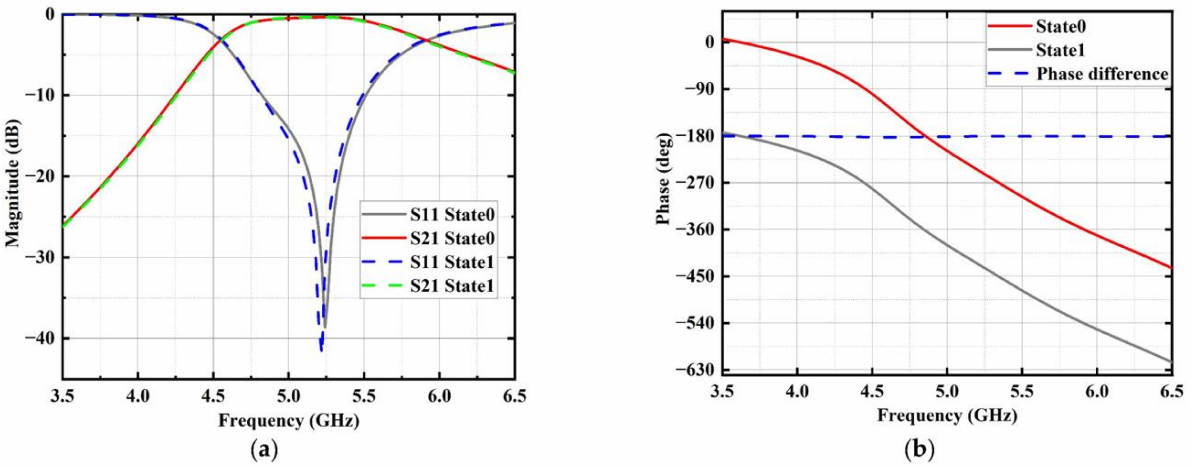

Figure 3.4.: Simulated (a) transmission (S_{21}) and reflection amplitude (S_{11}) and (b) phase response of the unit cell, demonstrating the 180° phase difference between the two states. From "A New 1 Bit Electronically Reconfigurable Transmitarray" [15].

Active devices such as PIN diodes require a DC biasing network. To minimize adverse effects on the electromagnetic performance, a narrow feeding network is integrated underneath the bottom metal grating using an additional dielectric layer (Rogers RO4450F). Figure 3.5 shows the optimized bias network layout that supplies with the required DC without significantly degrading the unit cell's transmission performance.

Once the definitive unit cell was designed, a 16×16 transmitarray was fabricated. The transmitarray is fed by a horn antenna and in order to achieve two-dimensional beam scanning, phase compensation must be applied to each unit cell. This is accomplished by appropriately setting the phase distribution ϕ_{mn}, which determines the radiation direction of the beam. The phase distribution for each unit cell is calculated using the following equation [13]:

$$\phi_{mn} = -k_0 \left(\left| \vec{R}_{mn} \right| - \vec{u}_0 \cdot \vec{r}_{mn} \right) + \Delta\phi$$

where:

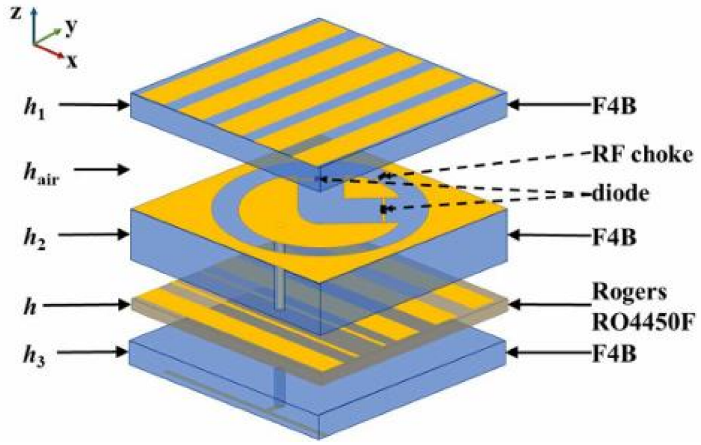

Figure 3.5.: Design of the unit cell including DC Bias Network. From "A New 1 Bit Electronically Reconfigurable Transmitarray" [15].

- ϕ_{mn} is the required phase distribution for the (m, n) unit cell.
- $k_0 = \frac{2\pi}{\lambda_0}$ is the free-space wavenumber, with λ_0 as the wavelength in free space.
- $\vec{R}_{mn}$ is the position vector from the phase center of the feed source to the (m, n) unit cell.
- $\vec{r}_{mn}$ is the position vector from the center of the transmitarray to the (m, n) unit cell.
- $\vec{u}_0$ is the direction vector of the desired transmission beam.
- $\Delta\phi$ is a constant representing the relative transmission phase. In this design, $\Delta\phi = 0$ is set for simplicity.

This phase distribution ensures that the signals from all unit cells are coherently combined in the desired beam direction, enabling precise control over the main lobe direction in both the azimuth and elevation planes.

Since the transmitarray uses 1-bit phase control, the continuous phase distribution calculated by the above equation must be quantized into two discrete states (0 or 180 degrees). The quantization is performed using the following coding scheme:

$$\phi_{qmn} = \begin{cases} 0^\circ, & \text{if } -90^\circ \leq \phi_{mn} < 90^\circ, \\ 180^\circ, & \text{otherwise,} \end{cases}$$

Here, ϕ_{qmn} is the quantized phase value applied to the (m, n) unit cell. This coding scheme effectively reduces the continuous phase distribution into 1-bit digital states suitable for the PIN-diode-based unit cells, facilitating dynamic beam scanning.

Once the 16×16 transmitarray prototype was fabricated, it was tested in an anechoic chamber to evaluate its performance. The prototype, shown in Figure 3.6, consists of the mentioned layers, and the necessary control circuitry for dynamic phase adjustment. The transmitarray is illuminated by a horn antenna positioned at a focal distance optimized for ensuring uniform illumination across the array.

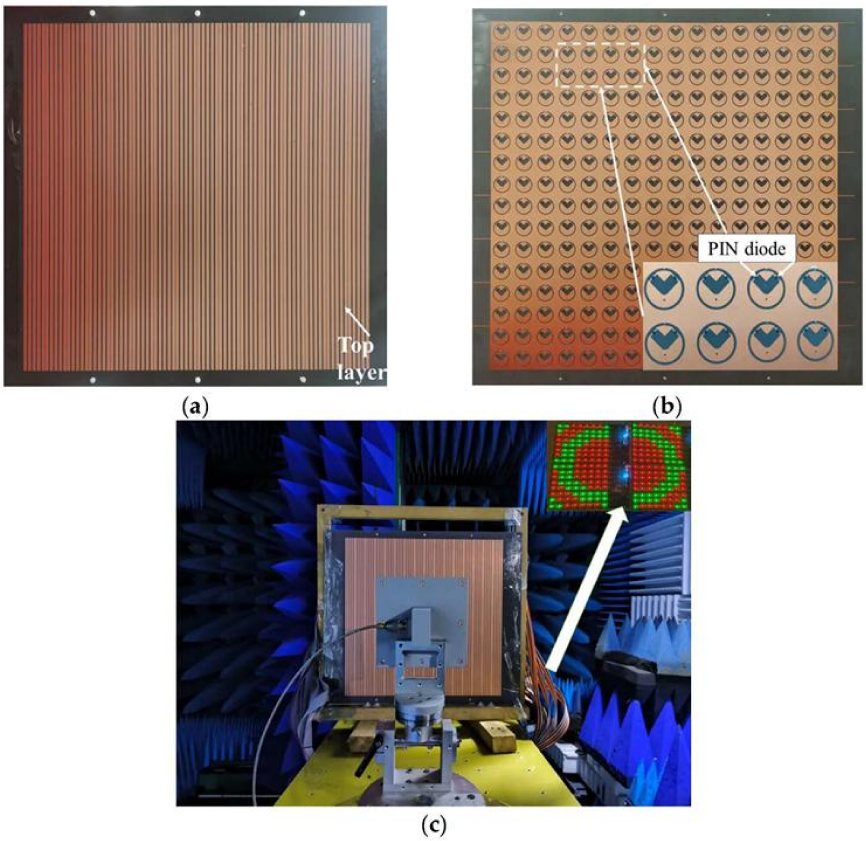

Figure 3.6.: Fabricated 16×16 transmitarray prototype and experimental setup in the anechoic chamber. (a) Top layer. (b) Middle layer. (c) Experimental setup. From [15].

The simulated and measured radiation patterns (Figure 3.7 and Figure 3.8) confirm that the transmitarray achieves two-dimensional beam scanning up to ±45° in both the E- and H-planes.

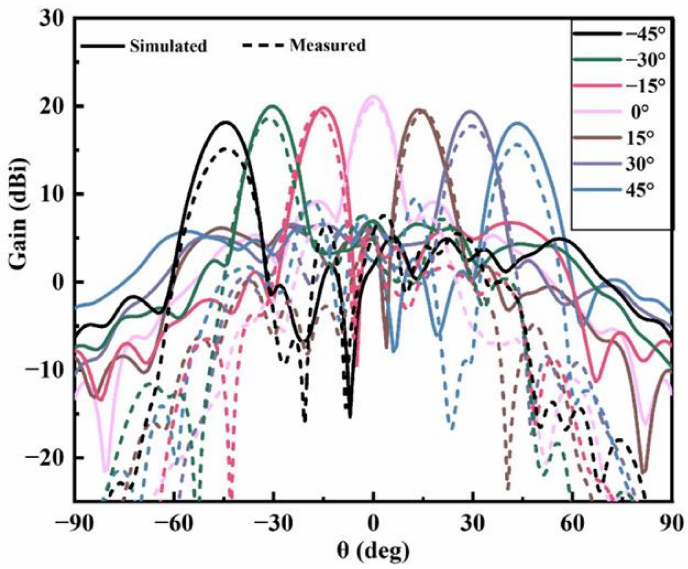

Figure 3.7.: Simulated and measured E-plane radiation pattern at 5 GHz for various beam scanning angles. From "A New 1 Bit Electronically Reconfigurable Transmitarray" [15].

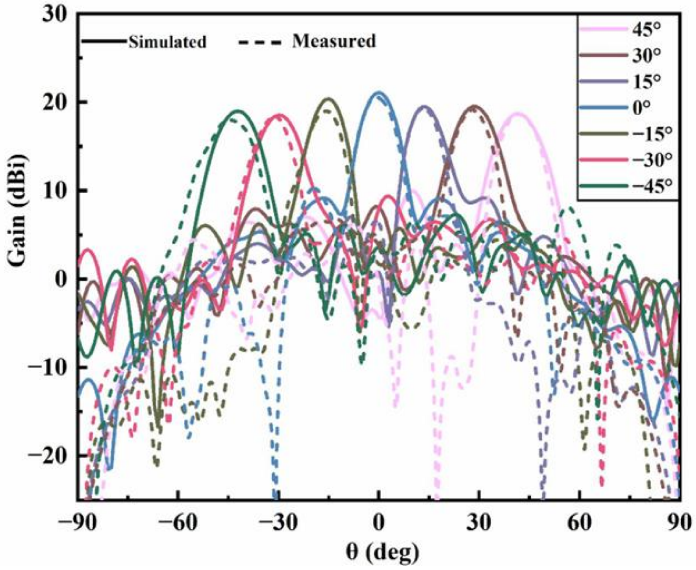

Figure 3.8.: Simulated and measured H-plane radiation pattern at 5 GHz for various beam scanning angles. From "A New 1 Bit Electronically Reconfigurable Transmitarray" [15].

CHAPTER 4

RIS Modeling and Simulation using CST STudio

"We can only see a short distance ahead,
but we can see many things that need to be done."
— Alan Turing, *1912-1954*.

4.1. Introduction to the CST Studio Simulator

CST Studio Suite is a comprehensive electromagnetic simulation software widely used for analyzing a broad spectrum of applications, including antenna design, electromagnetic compatibility (EMC), and wave propagation. It integrates multiple numerical methods, such as the Finite Integration Technique (FIT), the Finite Element Method (FEM), and the Transmission Line Matrix (TLM) method, allowing for precise simulations of complex 3D structures, lossy materials, and intricate electromagnetic environments. The software is particularly beneficial for antenna and RF design, microwave component simulation, and electromagnetic interference (EMI) analysis [16].

Figure 4.1.: CST Studio Suite Logo

One of the key features of CST Studio Suite, crucial for this project, is its ability to simulate unit cells and then assemble them into a Reconfigurable Intelligent Surface (RIS) array. This capability allows engineers to analyze and optimize the electromagnetic behavior of individual unit cells before scaling up to full RIS structures. The software provides accurate simulations of the electromagnetic response of these elements, enabling the design of advanced metasurfaces for applications such as beamforming, signal enhancement, and wireless communications.

CST Studio is extensively used across industries such as telecommunications, aerospace, automotive, and biomedical engineering. It enables engineers and researchers to design and optimize high-frequency systems efficiently by simulating the interaction of electromagnetic waves with conductors, dielectric materials, and intricate geometries. The software supports time-domain and frequency-domain solvers, making it suitable for applications like satellite communications, radar systems, and high-speed electronics.

One of CST Studio's key advantages is its intuitive graphical user interface, which simplifies the modeling and visualization of electromagnetic phenomena. Additionally,

it offers powerful post-processing tools for analyzing field distributions, antenna radiation patterns, and scattering parameters. The software also supports automation and optimization features, enhancing design workflows and enabling users to achieve optimal performance in their electromagnetic applications.

4.2. Unit Cell: design and simulation

The design of the unit cell for the reconfigurable intelligent surface (RIS) presented in this work is based on the unit cell proposed in "A 2-bit Tunable Unit Cell for 6G Reconfigurable Intelligent Surface Application" [22]. The original design consists of a split-ring resonator (SRR) loaded with a varactor diode, enabling tunability in the reflection phase response. As a starting point, the structure from [22] was adopted; however, some modifications have been introduced in this implementation. The most significant change is the choice of the dielectric substrate: instead of using Rogers RO3003, this work employs FR4 as the substrate material due to its availability and cost-effectiveness. While FR4 has a higher loss tangent compared to RO3003, it still provides adequate performance for the intended application.

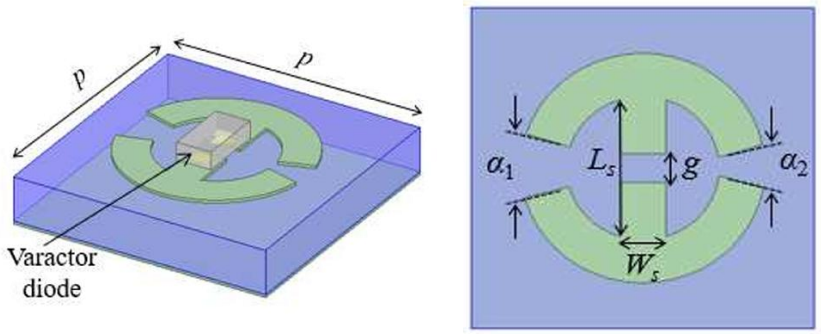

(a) Perspective view (b) Top view

Figure 4.2.: Geometrical design of the 2-bit tunable unit cell. From "A 2-bit Tunable Unit Cell for 6G Reconfigurable Intelligent Surface Application" [22]

4.2.1. Unit Cell Dimensions

The dimensions of the proposed unit cell are summarized in Table 4.1. These parameters were optimized to operate around 26.5 GHz, ensuring proper phase shifting and reflection magnitude.

Table 4.1.: Unit Cell Dimensions

Parameter	Value (mm)/(deg)
Periodicity (p)	3.0
Split-ring width (Ws)	0.4
Split width (g)	0.26
Substrate thickness (t)	1.6
Outer radius of SRR (R)	1.28
Angle α_1	32.25°
Angle α_2	21.52°

4.2.2. Varactor Model and Equivalent Circuit

To achieve the tunability required for the RIS unit cell, this work employs the MACOM MAVR-000120-1141 varactor diode [11]. This component provides a capacitance tuning range suitable for achieving a 2-bit quantized phase shift with approximately 90° steps. The equivalent circuit of the varactor is represented in Figure 4.3, where the capacitance varies depending on the applied bias voltage. The lumped element model used in the CST Studio simulation incorporates this values.

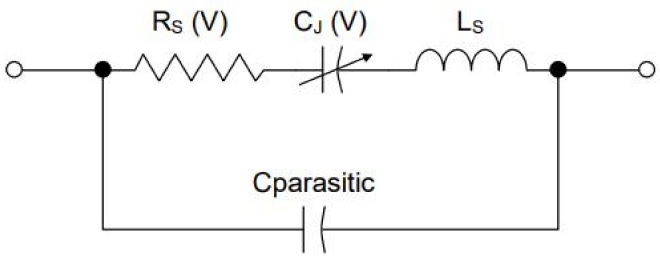

Figure 4.3.: Equivalent circuit model of the MAVR-000120-1141 varactor diode.

The equivalent parameters of the varactor, including series resistance and inductance, are shown in Table 4.2. These values were used to model the lumped RLC boundary in CST Studio.

Bias Voltage (V)	Series Inductance (nH)	Series Resistance (Ω)	Capacitance (pF)
0	0.02	1.07	0.9
1.5	0.02	1.06	0.68
3	0.02	1.06	0.54
5	0.02	1.04	0.43
7	0.02	1.01	0.36
10	0.02	0.93	0.29
14	0.02	0.74	0.23

Table 4.2.: Equivalent Circuit Parameters of the MAVR-000120-1141 Varactor

For achieving a 2-bit phase quantization, the capacitance values selected are: 0.9 pF, 0.38 pF, 0.31 pF, and 0.23 pF. These values allow a near 90° phase shift between quantization levels.

4.2.3. Simulation Results in CST Studio

The design was simulated in CST Studio Suite to evaluate its phase response and reflection amplitude at 26.5 GHz, slightly shifted from the original 24.5 GHz in [22]. The results indicate that the unit cell provides a nearly 90° phase shift between states while maintaining a balanced reflection amplitude across all configurations.

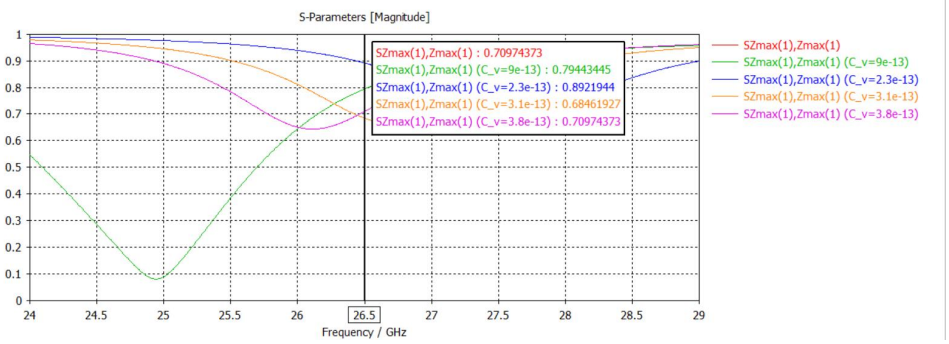

Figure 4.4.: Simulated reflection amplitude for different varactor bias voltages at 26.5 GHz.

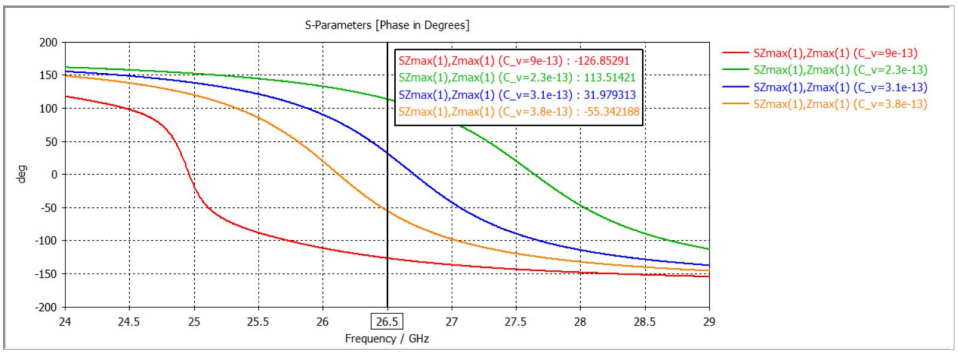

Figure 4.5.: Simulated reflection phase shift for different varactor bias voltages at 26.5 GHz.

As observed in Figures 4.4 and 4.5, at 26.5 GHz, the reflection amplitude remains relatively stable across all states, while the phase response exhibits a near 90° shift between quantization levels. This confirms the effectiveness of the proposed design for RIS applications.

4.2.4. Fabrication and Simulation Process (Appendix B)

The full process for constructing and simulating the unit cell in CST Studio is detailed in Appendix B.

4.3. RIS: Simulation and discussion

This section explains the key factors of the complete RIS array and present the results obtained from the simulations. The full process of the design and simulation of the RIS in CST Studio is detailed in the appendix B.

4.3.1. Array Dimensions

The RIS array is designed as a 32 x 32 matrix, resulting in a total of 1024 elements. The overall dimensions of the array are 96 x 96 mm, with the periodicity of the unit cells set to 3 mm, as derived from the unit cell design.

To provide a comparison with the wavelength (λ), we can calculate the array's dimensions in terms of the wavelength at the operating frequency of 26,5 GHz. The wavelength in free space is given by:

$$\lambda = \frac{c}{f}$$

where c is the speed of light (3×10^8 m/s) and $f = 26{,}5\,\text{GHz}$ is the frequency. Therefore, the wavelength is:

$$\lambda = \frac{3 \times 10^8\,\text{m/s}}{26{,}5 \times 10^9\,\text{Hz}} = 0{,}01132\,\text{m} = 11{,}32\,\text{mm},$$

With this, the total size of the array in terms of wavelength is:

$$\text{Array size in terms of } \lambda = \frac{96\,\text{mm}}{11{,}32\,\text{mm}} \approx 8{,}47\,\lambda,$$

This is a reasonable size for RIS arrays, as it allows for efficient beam steering and control while keeping the array compact enough to ensure manageable computational load in simulation. Such a size is consistent with other RIS implementations found in literature, such as [14] or [21], where arrays of similar dimensions (9.5 × 9.5 and 6.12 × 6.12 in terms of λ, respectively) were employed.

The array's size is large enough to achieve good performance in terms of beam steering and signal enhancement, and at the same time, it is small enough to not exceed the computational capacity of the PC used for simulations.The top and side views of the RIS array, as designed in CST Studio, are shown in Figures 4.6 and 4.7, respectively.

4.3.2. Coding Employed in the Simulations

For a beam steering application, it is common to utilize the phase distribution formula introduced in Section 3.2, which is derived from [24]. Specifically, the required phase for the (m, n) unit cell is determined by:

$$\phi_{mn} = -k_0 \left(\left| \vec{R}_{mn} \right| - \vec{u}_0 \cdot \vec{r}_{mn} \right) + \Delta\phi$$

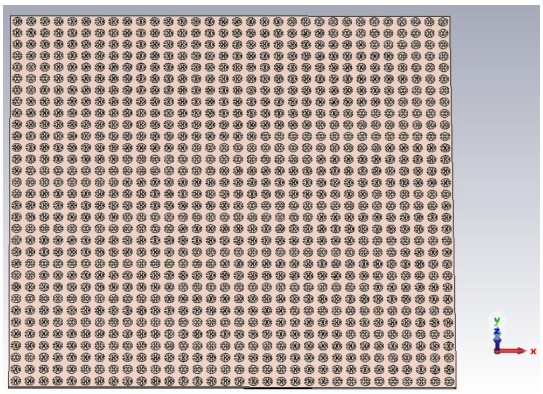

Figure 4.6.: Top view of the RIS array designed in CST Studio.

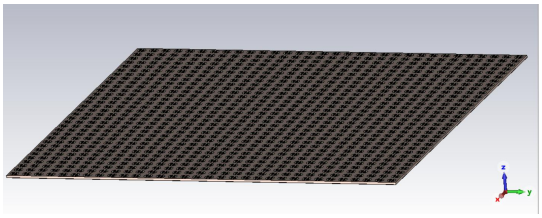

Figure 4.7.: Side view of the RIS array designed in CST Studio.

where:

- ϕ_{mn} is the required phase distribution for the (m, n) unit cell.
- $k_0 = \frac{2\pi}{\lambda_0}$ is the free-space wavenumber, with λ_0 as the wavelength in free space.
- $\vec{R}_{mn}$ is the position vector from the phase center of the feed source to the (m, n) unit cell.
- $\vec{r}_{mn}$ is the position vector from the center of the transmitarray to the (m, n) unit cell.
- $\vec{u}_0$ is the direction vector of the desired transmission beam.
- $\Delta\phi$ is a constant representing the relative transmission phase. In this design, $\Delta\phi = 0$ is set for simplicity.

This formula is implemented to dynamically assign the phase settings to each unit cell, ensuring accurate beam steering.

Following this, a quantization process should be applied, similar to the approach used in Section 3.2, but adapted to the four possible states of the unit cell. In this case, the quantized phase is given by:

$$\phi_{qmn} = \begin{cases} 0^\circ, & \text{if } -45^\circ \leq \phi_{mn} < 45^\circ, \\ 90^\circ, & \text{if } 45^\circ \leq \phi_{mn} < 135^\circ, \\ 180^\circ, & \text{if } \phi_{mn} \geq 135^\circ \text{ or } \phi_{mn} < -135^\circ, \\ 270^\circ, & \text{if } -135^\circ \leq \phi_{mn} < -45^\circ, \end{cases}$$

This quantization allows the phase distribution to be mapped to the discrete states supported by the 2-bit tunable unit cell, ensuring proper beam steering while maintaining the simplicity of the design.

However, in this case, as done in some research articles, one of the most common codings will be applied, and the RIS's effect on beam steering will be observed experimentally. Specifically, a linear coding scheme is used, where the states alternate by columns according to the periodicity defined by N, as illustrated in Figure 4.8, 4.9, 4.10 and 4.11.

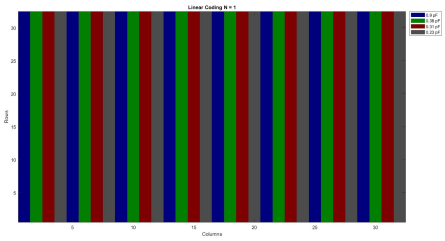

Figure 4.8.: Linear Coding with $N = 1$.

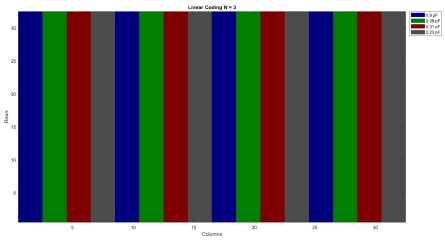

Figure 4.9.: Linear Coding with $N = 2$.

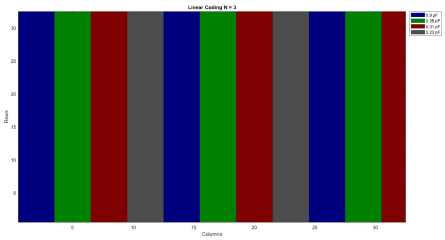

Figure 4.10.: Linear Coding with $N = 3$.

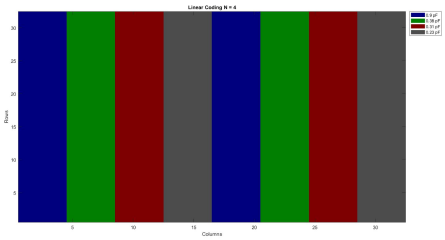

Figure 4.11.: Linear Coding with $N = 4$.

Experiments will be conducted with $N = 1, 2, 3$, and 4 to analyze how different periodicities influence the beam steering behavior. This approach allows for an empirical assessment of the RIS's effectiveness in modifying the beam direction.

4.3.3. Excitation

In this simulation, the excitation is modeled as a plane wave with linear polarization. For each coding configuration, three different incidence angles are considered to simulate various practical scenarios where the RIS could operate. The three angles of incidence are: normal incidence, an incidence angle of 30° relative to the vertical axis, and an incidence angle of 60° relative to the vertical axis. These angles represent

common real-world conditions under which a RIS could be deployed for beamforming and signal enhancement.

The propagation vectors used for these incidence angles are calculated using the spherical coordinate transformation:

$$\vec{k} = (\sin\theta\cos\phi, \sin\theta\sin\phi, -\cos\theta)$$

where:

- θ is the elevation angle (angle with respect to the vertical axis),
- ϕ is the azimuthal angle,
- $\vec{k}$ is the propagation vector of the incident plane wave.

For the three considered incidence angles, the corresponding propagation vectors are:

- Normal incidence: $\vec{k} = (0, 0, -1)$,
- 30° incidence relative to the vertical axis: $\vec{k} = (0{,}5, 0, -0{,}866)$,
- 60° incidence relative to the vertical axis: $\vec{k} = (0{,}866, 0, -0{,}5)$.

These vectors are directly related to the angles θ (the angle with respect to the vertical axis) and ϕ (the azimuthal angle).

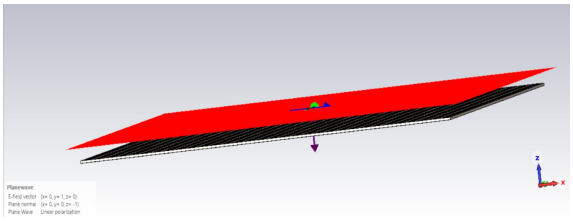

Figure 4.12.: Normal incidence of the plane wave in CST Studio.

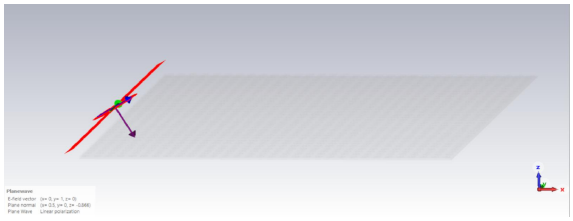

Figure 4.13.: Incidence at 30° with respect to the vertical in CST Studio.

As shown in Figures 4.12, 4.13 and 4.14 the plane wave incidence is simulated for normal, 30° and 60° angles relative to the vertical axis.

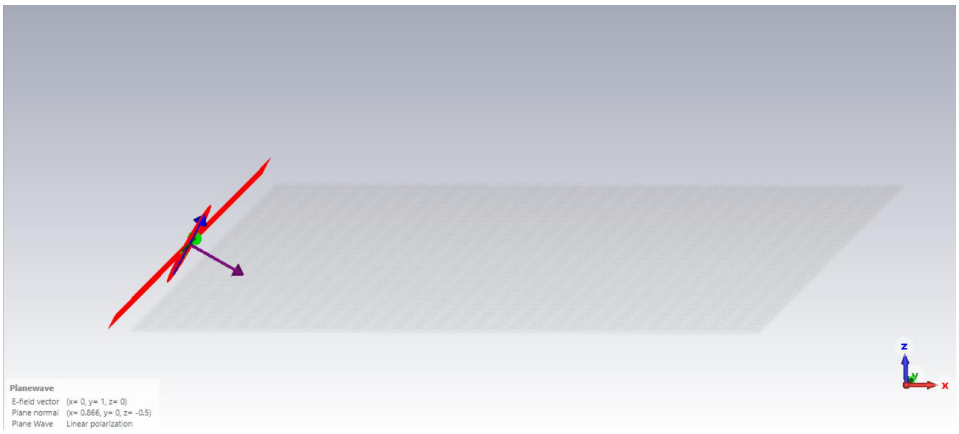

Figure 4.14.: Incidence at 60° with respect to the vertical in CST Studio.

4.3.4. Results

The results are presented as the RCS in dB/m^2, a crucial parameter for beam steering applications as introduced in Chapter 2. After simulating and comparing various RIS arrays already implemented, it was observed that the CST results are as expected, but an additional main lobe with considerable power appears in the specular direction of the incident plane wave; hence, for the purpose of evaluating the reflection angle of the RIS, this lobe is ignored in all simulations.

Below, the results for each coding configuration ($N = 1, 2, 3, 4$) are shown for three incidence angles (normal, 30°, and 60°). For each experiment, a 3D RCS plot and a 1D RCS plot are provided.

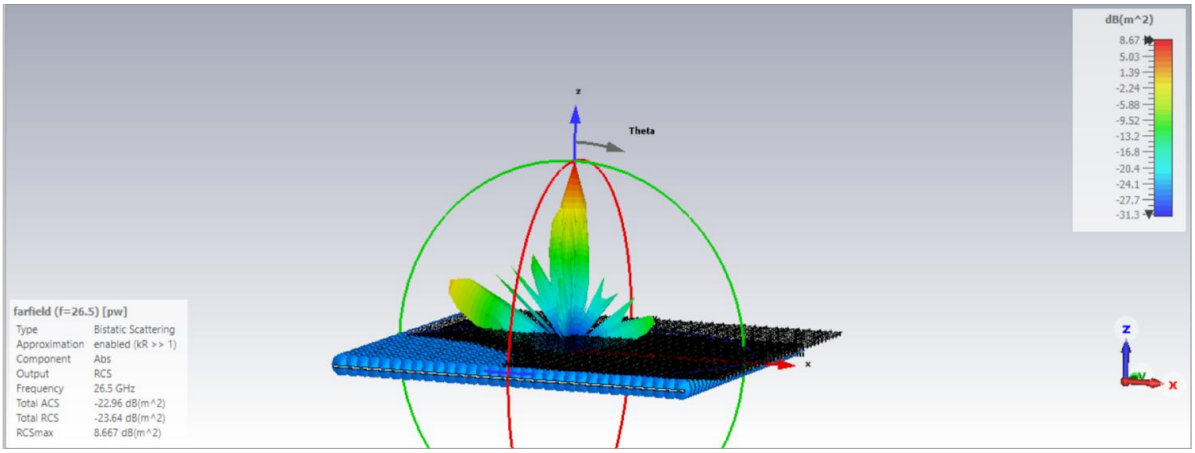

Figure 4.15.: 3D RCS for $N = 1$, normal incidence.

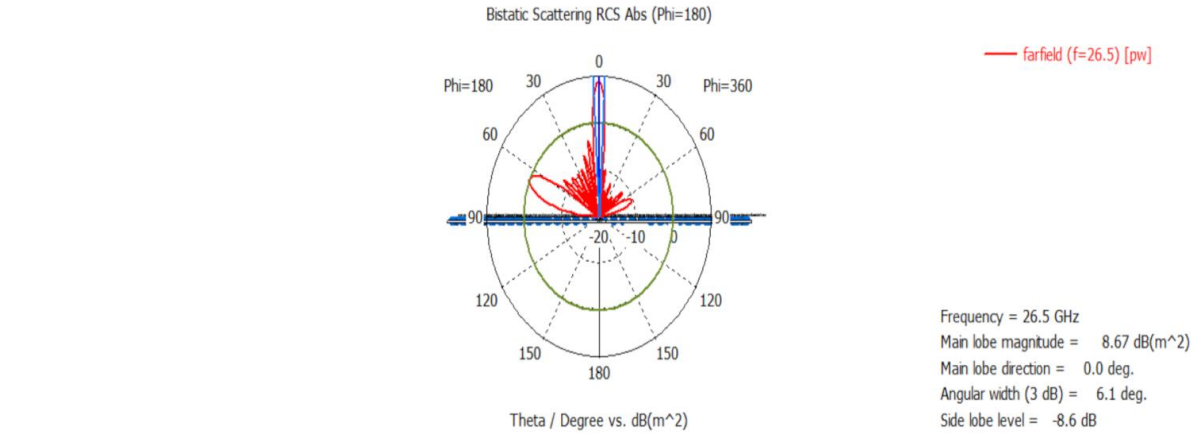

Figure 4.16.: 1D RCS for $N = 1$, normal incidence.

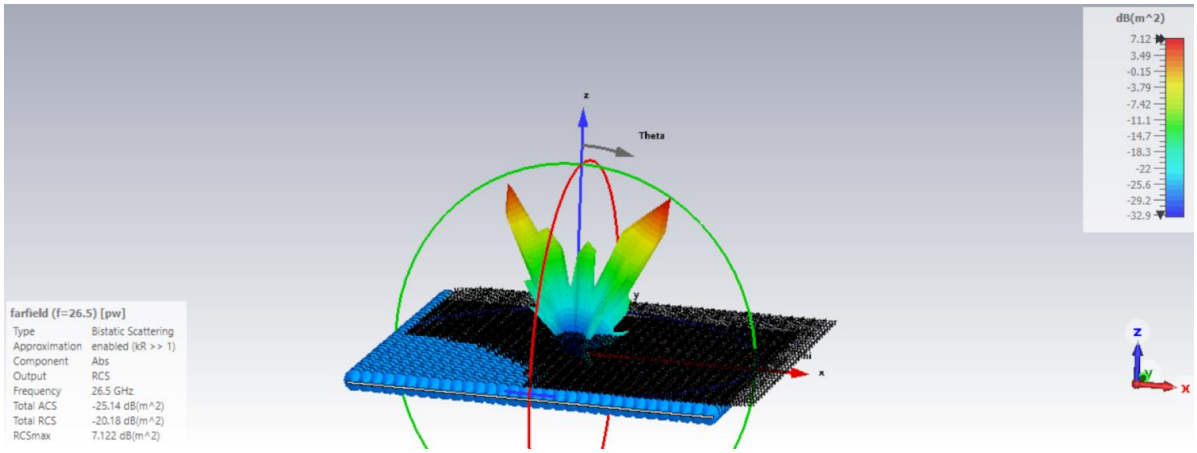

Figure 4.17.: 3D RCS for $N = 1$, 30° incidence.

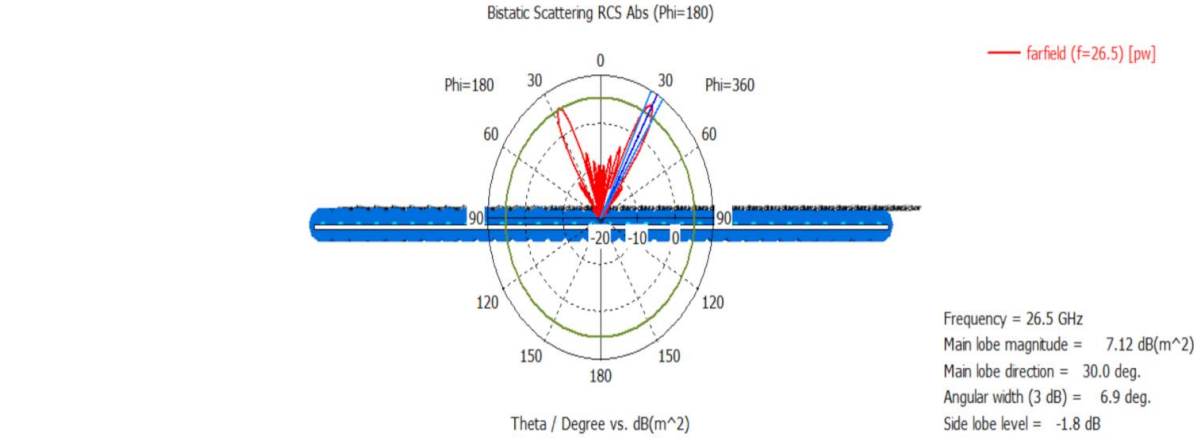

Figure 4.18.: 1D RCS for $N = 1$, 30° incidence.

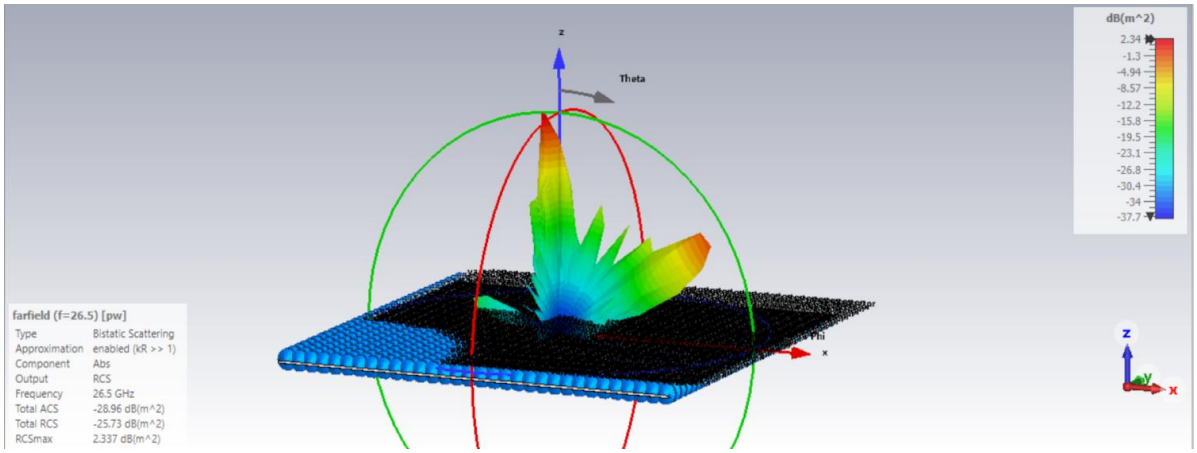

Figure 4.19.: 3D RCS for $N = 1$, 60° incidence.

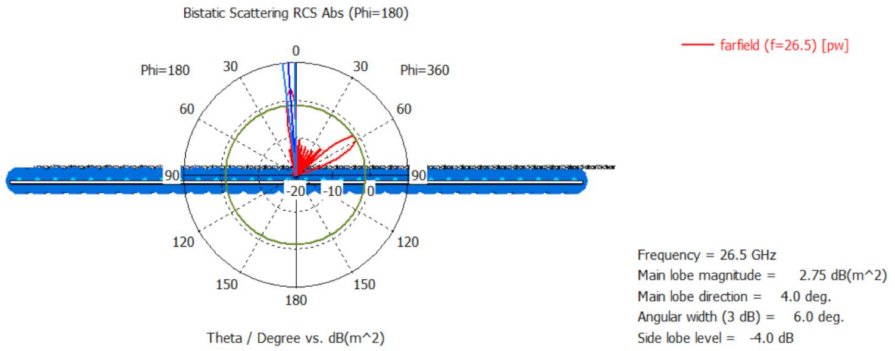

Figure 4.20.: 1D RCS for $N = 1$, 60° incidence.

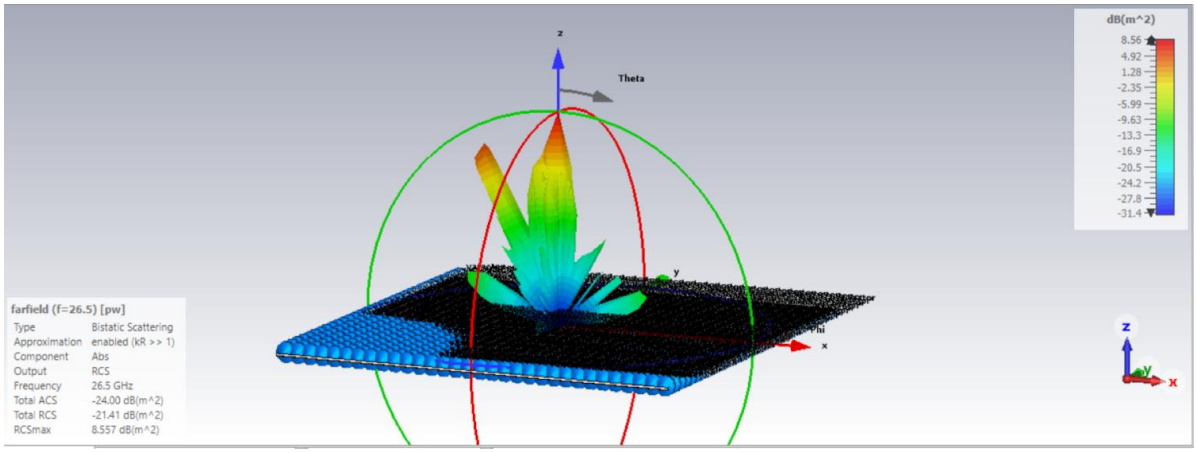

Figure 4.21.: 3D RCS for $N = 2$, normal incidence.

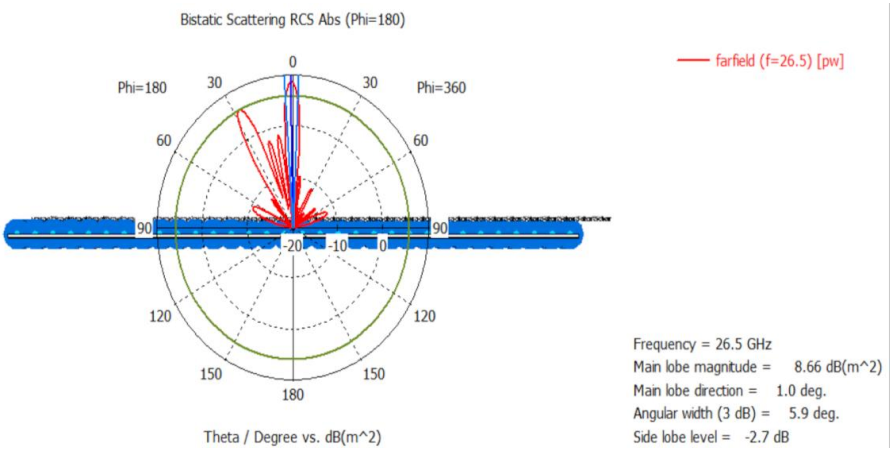

Figure 4.22.: 1D RCS for $N = 2$, normal incidence.

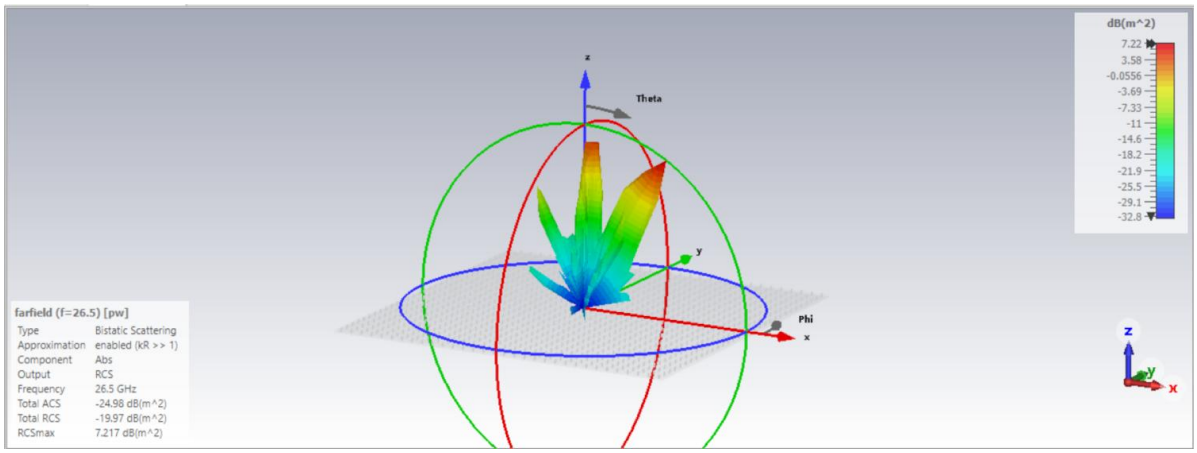

Figure 4.23.: 3D RCS for $N = 2$, 30° incidence.

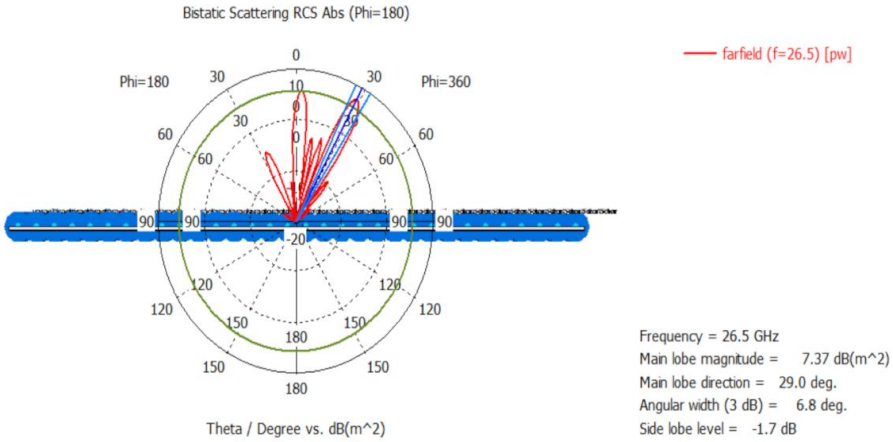

Figure 4.24.: 1D RCS for $N = 2$, 30° incidence.

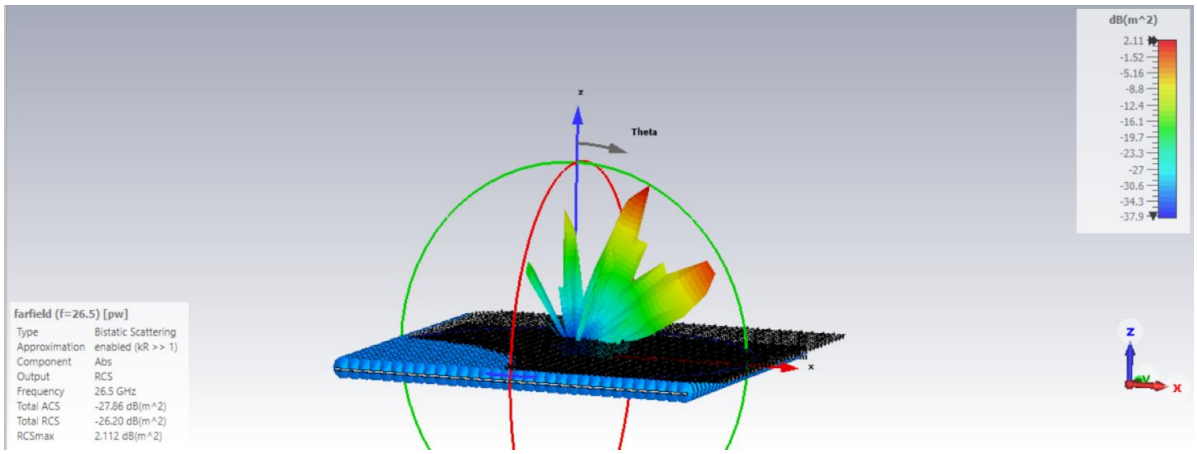

Figure 4.25.: 3D RCS for $N = 2$, 60° incidence.

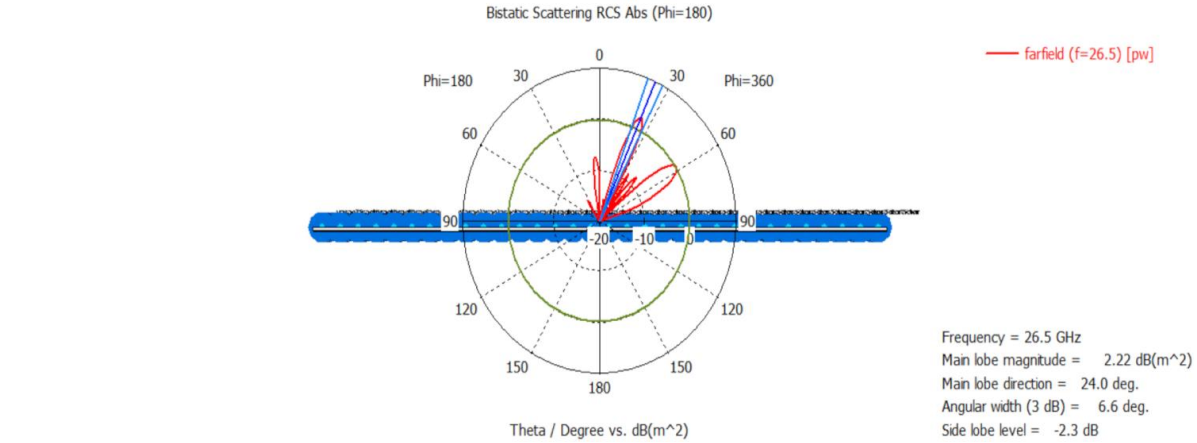

Figure 4.26.: 1D RCS for $N = 2$, 60° incidence.

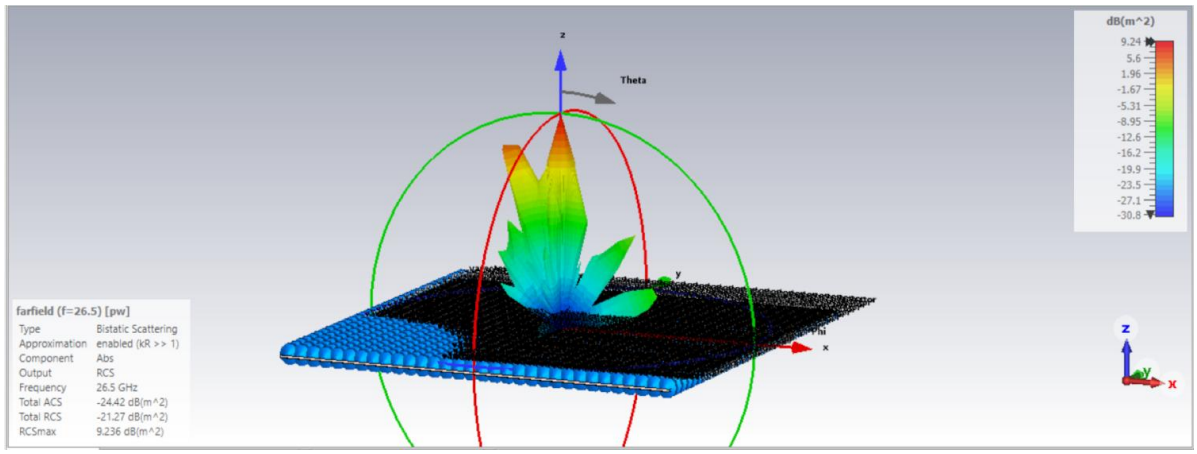

Figure 4.27.: 3D RCS for $N = 3$, normal incidence.

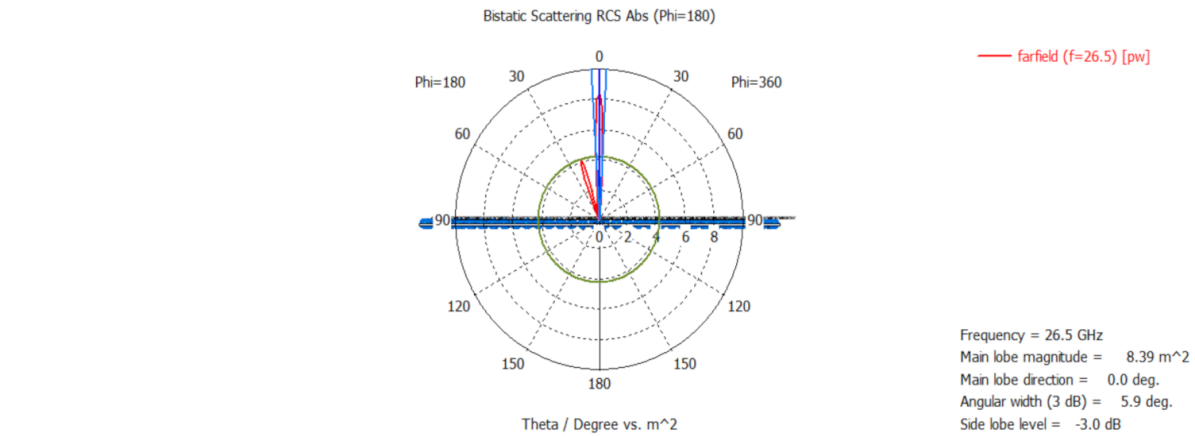

Figure 4.28.: 1D Linear RCS for $N = 3$, normal incidence.

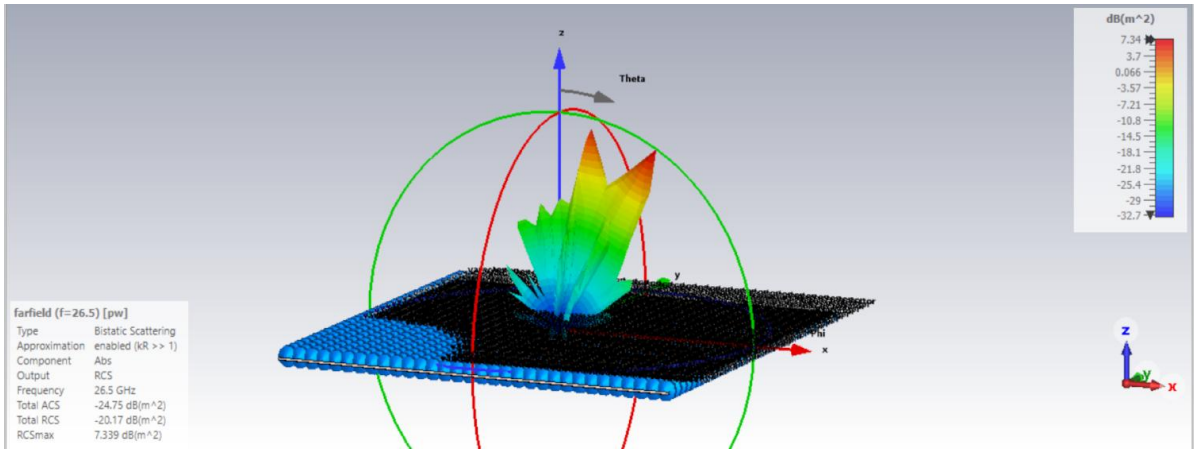

Figure 4.29.: 3D RCS for $N = 3$, 30° incidence.

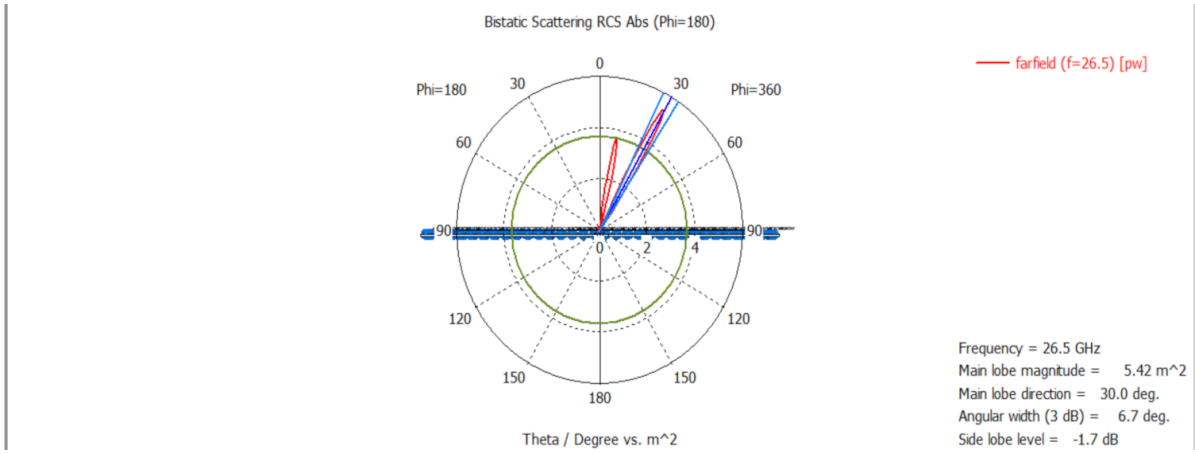

Figure 4.30.: 1D Linear RCS for $N = 3$, 30° incidence.

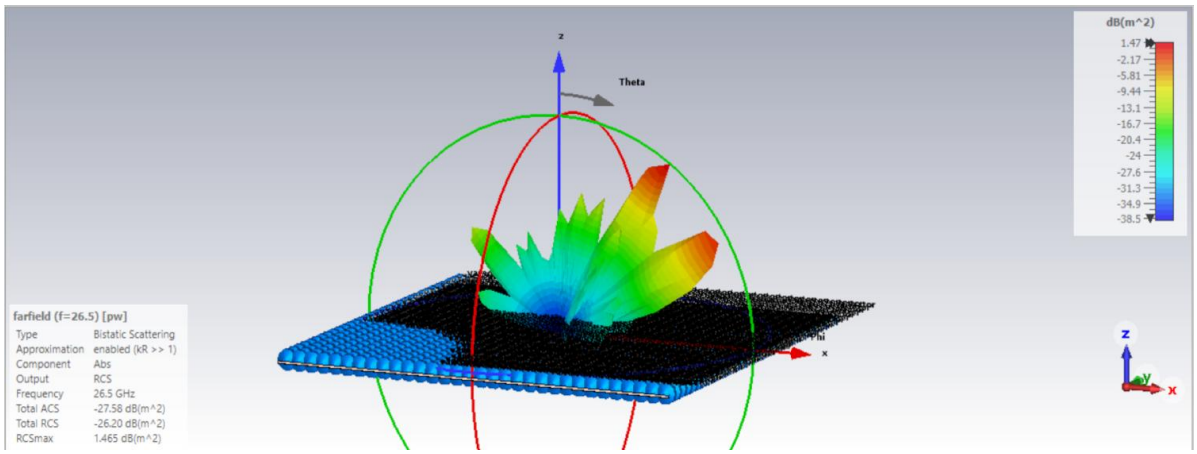

Figure 4.31.: 3D RCS for $N = 3$, 60° incidence.

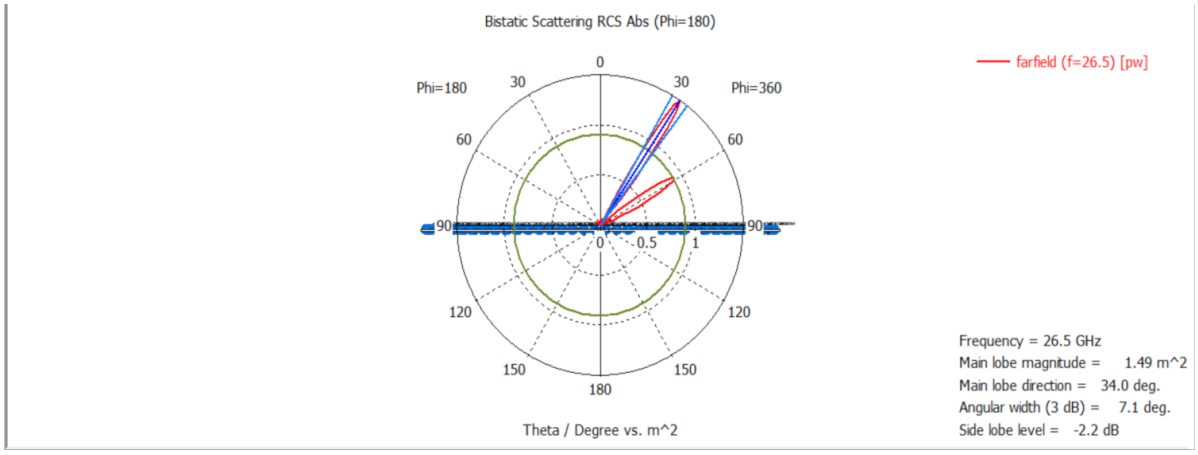

Figure 4.32.: 1D Linear RCS for $N = 3$, 60° incidence.

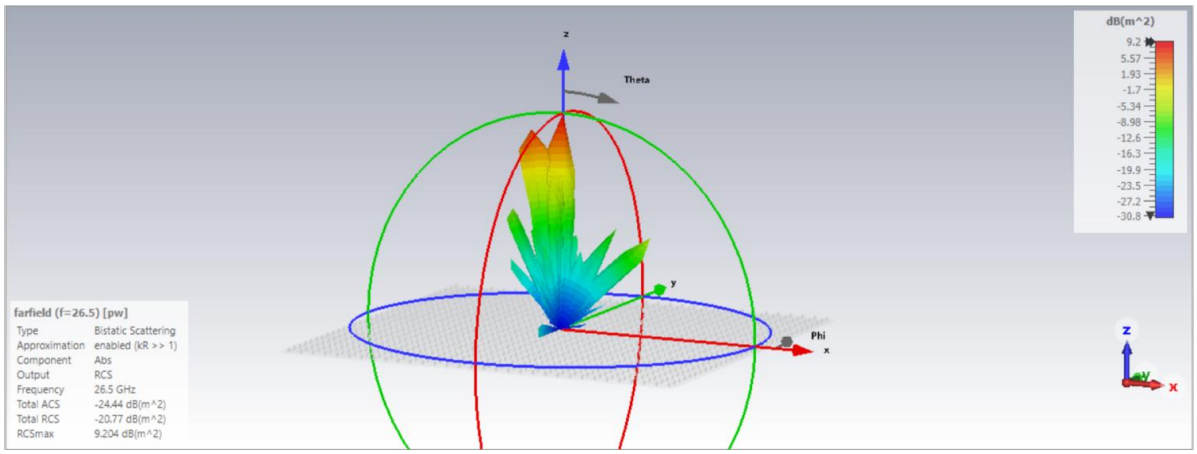

Figure 4.33.: 3D RCS for $N = 4$, normal incidence.

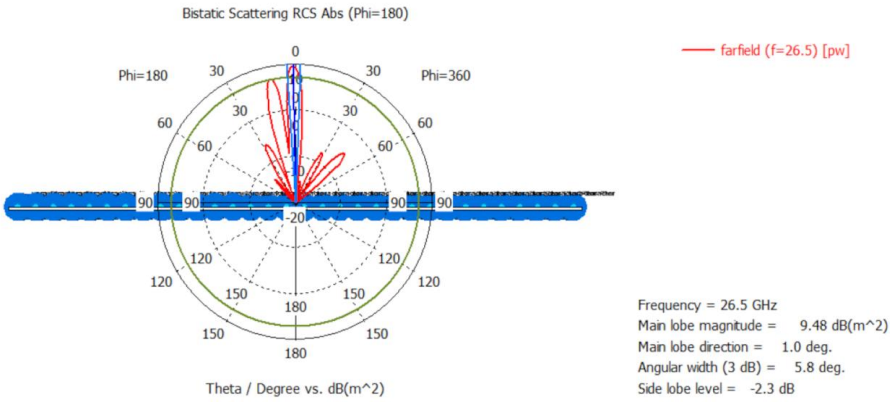

Figure 4.34.: 1D RCS for $N = 4$, normal incidence.

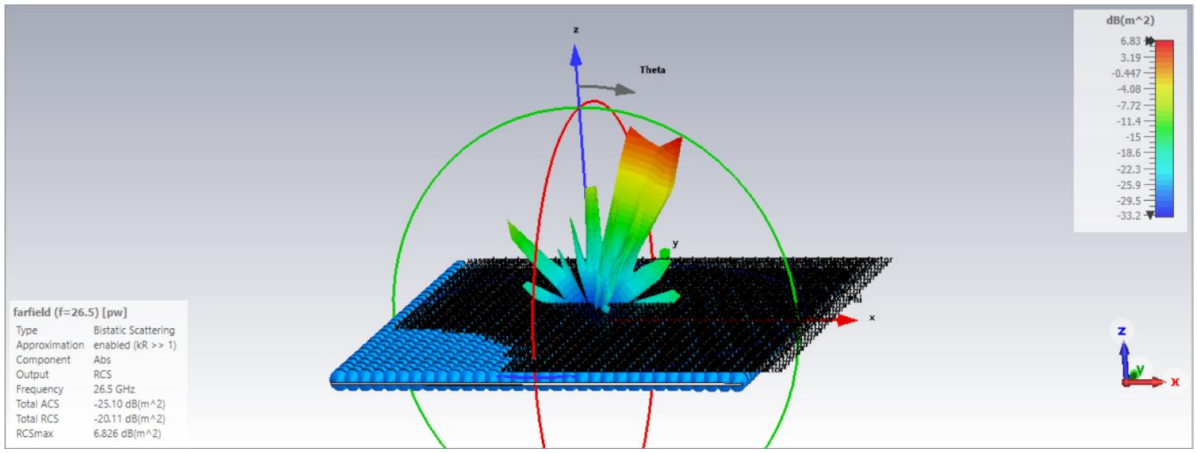

Figure 4.35.: 3D RCS for $N = 4$, 30° incidence.

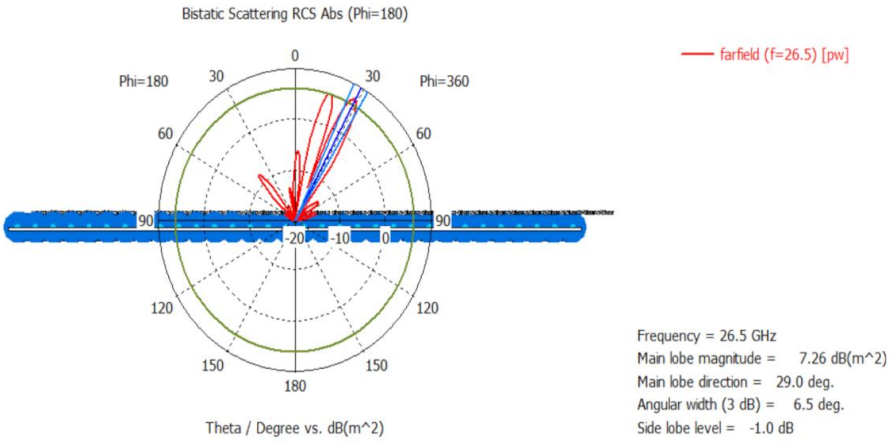

Figure 4.36.: 1D RCS for $N = 4$, 30° incidence.

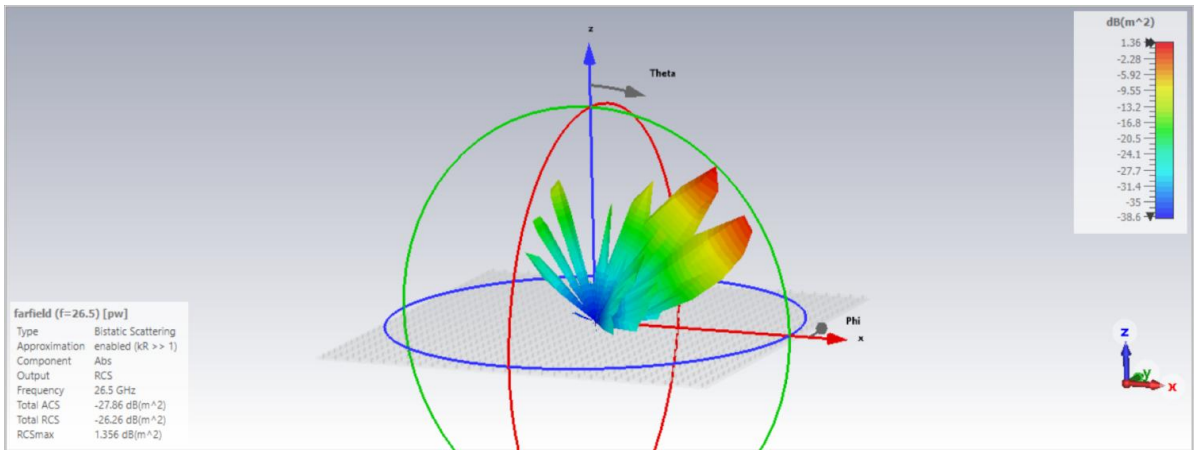

Figure 4.37.: 3D RCS for $N = 4$, 60° incidence.

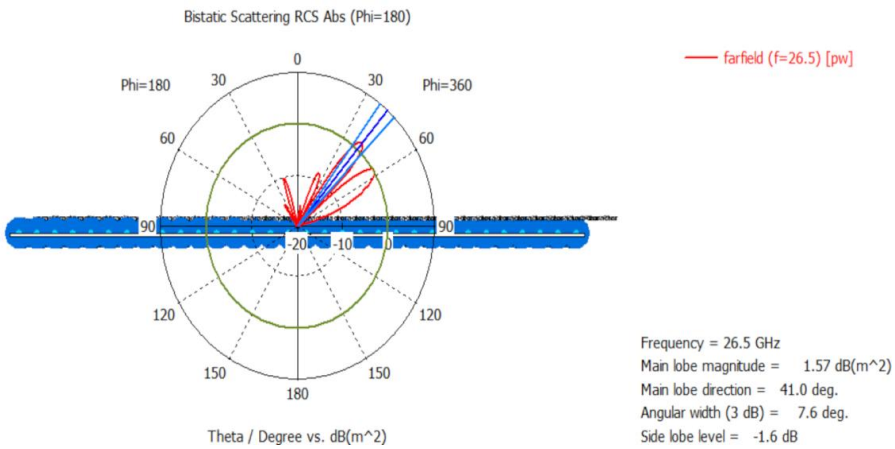

Figure 4.38.: 1D RCS for $N = 4$, 60° incidence.

Table 4.3 summarizes the reflected angle θ for the different coding configurations (N) and incidence angles, measured with respect to the vertical axis as shown in Figure 4.39. The reflected angle is obtained by analyzing the main beam direction in the 1D RCS plots (excluding the specular lobe).

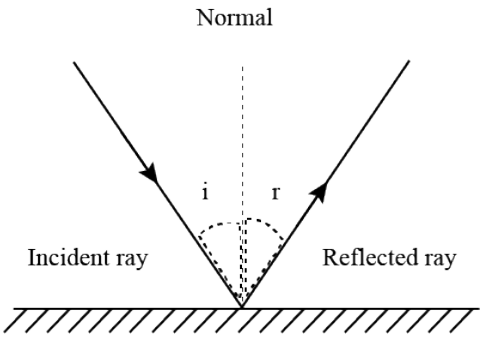

Figure 4.39.: Incidence and reflection angles measured with respect to the vertical axis.

Table 4.3.: Reflected angle θ for different coding configurations and incidence angles.

N	**Incidence Angle (θ_i)**	**Reflected Angle (θ_r)**
1	0°	-66°
	30°	-27°
	60°	-4°
2	0°	-28°
	30°	3°
	60°	24°
3	0°	-19°
	30°	11°
	60°	34°
4	0°	-12°
	30°	17°
	60°	41°

These results demonstrate that a reflective RIS has been successfully designed, which is effective in covering a wide angular range of reflection with the different linear encoding configurations and incident waves employed. These findings showcase the potential for applications in beam steering, where new encoding schemes can be implemented beyond those currently considered. An important observation is that the pattern followed by the linear codings used in our experiments shows a consistent

trend: the reflection angle shifts away from the specular direction in a decreasing manner with increasing N. In other words, the larger the N, the closer the reflected angle becomes to the specular reflection. Additionally, the angular distance from the specular reflection remains relatively stable for each encoding, regardless of the incidence angle, highlighting the predictable nature of the RIS design for beam steering purposes.

CHAPTER 5

CONCLUSIONS AND FUTURE WORK

"There are always things
worth living for."
— Jesús Quintero. *1940-2022*.

5.1. Overall Conclusions

This study has highlighted the critical role of Reconfigurable Intelligent Surfaces (RIS) in overcoming the challenges of terahertz communications in 6G networks. By enabling dynamic control of electromagnetic waves, RIS enhances signal strength, coverage, and energy efficiency, paving the way for more reliable and adaptive wireless communication systems.

The findings underscore the transformative potential of RIS in optimizing beamforming and mitigating propagation challenges inherent to high-frequency bands. As 6G technology continues to evolve, the strategic implementation of RIS will be

essential to achieving the goals of ultra-fast data rates, low latency, and seamless global connectivity.

Throughout this project, a complete design and simulation methodology for a Reconfigurable Intelligent Surface (RIS) was presented, addressing both the individual unit cell and the full array configuration. The choice of a 2-bit tunable unit cell allowed the RIS to demonstrate a broad range of reflection angles, verified through numerical simulations in CST Studio Suite. Different linear coding schemes were implemented to explore the beam steering capabilities, showing that the RIS can effectively redirect the reflected wave under various incidence angles. Additionally, it was confirmed that increasing the coding parameter N shifts the reflection angle closer to the specular direction, while the angular difference from the specular reflection remains relatively stable for each configuration, regardless of the angle of incidence.

The obtained results validate the effectiveness of the proposed RIS design for applications that require flexible beam control, such as wireless communication and radar systems. By confirming that the main lobe of the reflected beam can be accurately steered, this work highlights the potential of RIS technology for next-generation communication systems, including mm-Wave, 5G and beyond.

5.2. Future Work

Looking ahead, several lines of research and development arise:

- **Design and Simulation Including the Bias Network:** Incorporating the bias network into the electromagnetic simulation will provide a more realistic representation of the RIS. This includes modeling the varactor diodes bias lines and ensuring minimal interference with the RF performance.
- **Fabrication of a Prototype:** Building a physical RIS prototype based on the proposed design will enable experimental validation. PCB manufacturing techniques can be employed, with the commercial varactors and FR4 substrates the costs would be manageable.
- **Anechoic Chamber Measurements:** Once the prototype is fabricated, measurements in an anechoic chamber with horn antennas (transmitter and receiver) will allow precise evaluation of the RIS performance. By controlling the angles

of incidence and reflection, the experimental data can confirm and refine the simulation results.

- **FPGA-Based Control:** Implementing real-time control of the RIS phase distribution via an FPGA will enable rapid reconfiguration of the reflection angle. This setup would be particularly useful for dynamic beam steering scenarios, where the target user or object moves over time.
- **Artificial Intelligence for Beam Steering:** Integrating AI algorithms to predict user or object motion could further optimize the RIS reconfiguration. By forecasting changes in position or channel conditions, the system can adapt quickly and efficiently, enhancing the overall performance and reliability of the beam steering process.

In conclusion, the proposed RIS design serves as a strong foundation for further research and development. By extending the work to include bias network design, prototype fabrication, and experimental validation, the capabilities of the RIS can be thoroughly tested and improved. Moreover, incorporating advanced control techniques, such as FPGA-based reconfiguration and AI-driven beam steering, opens the door to even more sophisticated and dynamic applications in next-generation wireless systems.

APPENDIX A

Sixth Generation of Mobile Networks. 6G.

The sixth generation of mobile networks, known as 6G, is being developed to address the limitations of 5G and to meet the demands of emerging applications that require higher capacity, faster speeds, and improved performance. While 5G has significantly enhanced network capabilities, some critical applications—such as augmented reality, autonomous vehicles, telemedicine, and massive Internet of Things (IoT)—require even greater data rates, lower latency, and higher reliability. These needs exceed the current capabilities of 5G.

In addition to these technological requirements, 6G is also motivated by the explosive growth in the number of connected users and devices worldwide, as shown in the Figure A.1. This growth puts immense pressure on existing networks, making it clear that a new generation of technology is needed to support the increasing demand. 6G is designed to handle these vast amounts of traffic and to provide the necessary infrastructure to ensure reliable, high-speed connections for billions of users and devices [6].

The motivation for 6G lies in the need to provide more comprehensive global coverage, integrating not only terrestrial communication but also air, sea, and space-based systems. The future of communications envisions networks capable of seamless connectivity across different environments, ensuring that no area is left uncovered. Moreover, as sustainability and energy efficiency become increasingly important,

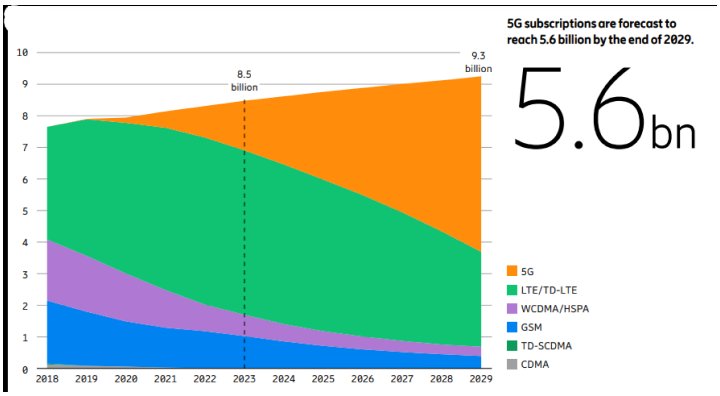

Figure A.1.: Mobile subscriptions by technology (billion)

6G technologies are focusing on reducing carbon footprints and improving energy consumption through more eco-friendly solutions.

A.1. Roadmap and Timeline

The development of 6G follows the historical trend of mobile network generations, with new generations typically emerging every decade. 6G is currently in the pre-standardization phase, with key developments taking place by the end of 2023. In March 2024, 3GPP committed to a formal timeline for 6G development, as shown in the Figure A.2, starting with Release 19, which will focus on use cases and initial requirements. Technical studies will begin with Release 20, and the first 6G specifications are expected by the end of 2028 in Release 21 [5].

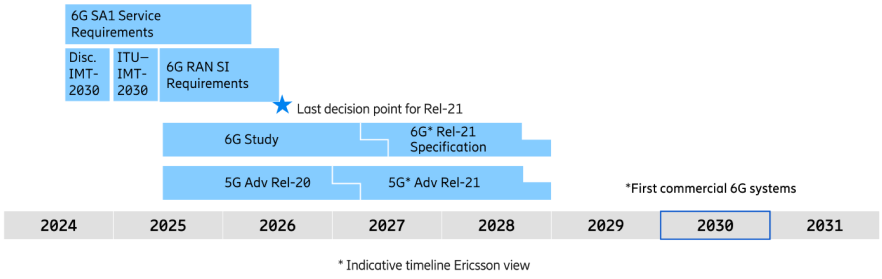

Figure A.2.: 3GPP timeline

The International Telecommunication Union (ITU), which oversees global telecom standards, has designated 6G as IMT-2030. ITU will define performance requirements from 2024 to 2026 and will evaluate technology submissions between 2027 and 2029 [5].

Figure A.3.: ITU Timeline

The goal is for the first commercial 6G deployments to begin by 2030, aligning with the ITU and 3GPP timelines.

A.2. Architecture and Key Technologies

The architecture of 6G is expected to go beyond traditional terrestrial networks, incorporating a fully integrated communication system that combines terrestrial, aerial, satellite, and underwater networks, as shown in Fig A.4. This convergence will ensure global and ubiquitous coverage, enabling continuous connectivity across diverse environments.

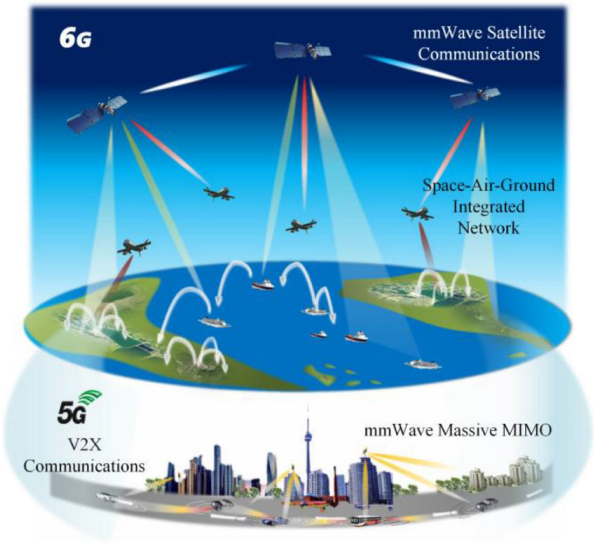

Figure A.4.: Conceptual illustration of the 6G communication network that encompasses the 5G network.

Key enabling technologies for 6G include the use of new frequency bands such as the THz spectrum, which offers vast bandwidth potential for ultra-fast data transmission. Additionally, visible light communication (VLC) and the objective of this project,

Reconfigurable Intelligent Surfaces (RIS) are emerging as breakthrough technologies that will enhance spectrum efficiency and signal propagation. Artificial intelligence (AI) and machine learning (ML) will also play a central role in network optimization, enabling predictive resource allocation, self-organizing networks, and real-time decision-making processes.

6G will also integrate sensing capabilities, enabling networks to not only communicate but also perceive and interact with the environment. This integration of communication and sensing will drive new applications in areas such as smart cities, healthcare, and environmental monitoring.

A.3. Spectrum and Frequency Bands

One of the key differences between 6G and previous generations is the use of higher frequency bands. While 5G has already started exploring millimeter-wave (mmWave) frequencies, 6G will push further into the THz range (0.1-10 THz), unlocking significantly more bandwidth and supporting data rates up to 1 Tbps. These higher frequencies, however, come with challenges, such as limited range and penetration capabilities, requiring new network designs that utilize intelligent surfaces and reconfigurable materials to direct and amplify signals.

In addition to THz frequencies, 6G will leverage a wide range of spectral resources, including sub-6 GHz, mmWave, and visible light, to ensure network flexibility and adaptability. The use of these bands will enable 6G to support a vast array of applications with varying requirements, from high-speed internet for urban centers to low-power, long-range connectivity for remote areas.

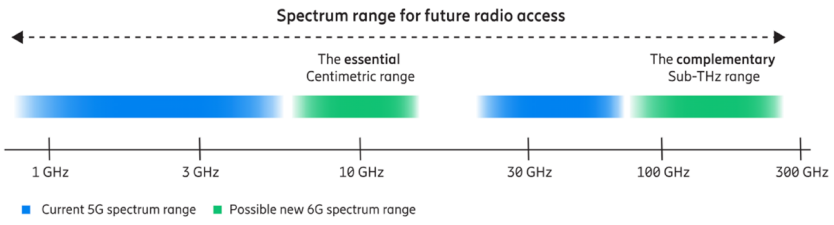

Figure A.5.: Spectrum range for 6G

A.4. New Applications and Use Cases

As we transition from the capabilities of 5G to the transformative potential of 6G, a myriad of new applications and use cases are emerging that promise to reshape industries, enhance user experiences, and address global challenges. This evolution is evident in the progression from 5G's key service categories—Ultra-Reliable Low Latency Communication (URLLC), Enhanced Mobile Broadband (eMBB), and massive Machine Type Communications (mMTC)—to their enhanced versions in 5G Advanced (5GA) and the revolutionary services enabled by 6G.

The Fig A.6 illustrating the evolution from 5G to 5G Advanced and subsequently to 6G highlights this shift. While 5G laid the groundwork for high-speed connectivity and low latency, 5G Advanced introduced enhancements in existing use cases, such as improved performance for critical applications. As we move into the 6G era, we can anticipate a broad spectrum of new and innovative applications that leverage advanced capabilities, such as AI-driven services, critical communications for emergency response, and immersive experiences that integrate augmented and virtual reality.

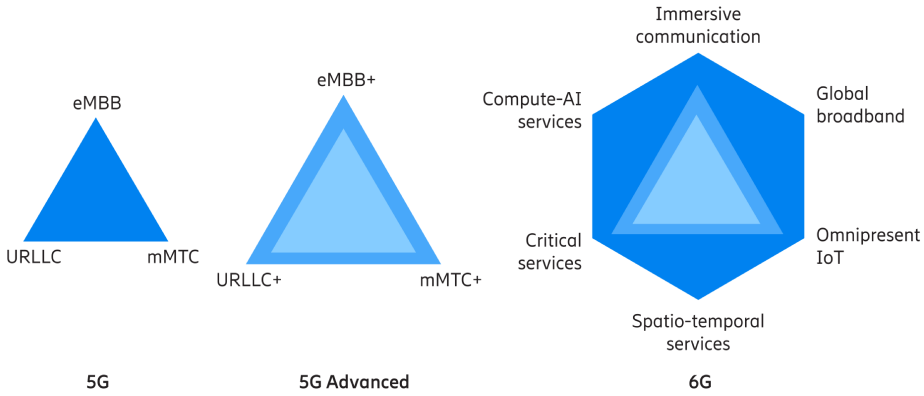

Figure A.6.: Growing from 5G to 6G

As shown, the advent of 6G will enable a variety of groundbreaking applications, including:

1. Compute AI-Services: The integration of artificial intelligence directly into the network infrastructure will enable real-time data processing and decision-making at the edge. This capability will enhance applications in autonomous systems, predictive maintenance, and personalized user experiences across various sectors, including healthcare, manufacturing, and transportation.

2. Critical Services: 6G is poised to support a new level of reliability and latency requirements, crucial for mission-critical applications such as remote surgeries, autonomous vehicles, and disaster management systems. The ability to provide deterministic latency and guaranteed reliability will make these services feasible and safe.

3. Spatio-Temporal Services: The advancement in spatial and temporal awareness will enable applications such as smart cities and advanced navigation systems. By understanding the context of users and devices in real-time, 6G can facilitate efficient resource management, traffic optimization, and enhanced urban planning.

4. Immersive Communication: With the rise of virtual and augmented reality technologies, 6G will enable seamless immersive communication experiences. Users will interact in shared virtual spaces, enhancing remote collaboration, social interaction, and entertainment. This will transform sectors like education, gaming, and virtual tourism.

5. Omnipresent IoT: The expansion of the Internet of Things (IoT) will reach new heights with 6G, providing connectivity to an unprecedented number of devices. This omnipresence will enable smart homes, healthcare monitoring systems, and industrial automation on a global scale, driving efficiency and innovation.

6. Global Broadband: 6G aims to provide ubiquitous broadband connectivity, bridging the digital divide in underserved regions. With global coverage, high data rates, and low latency, 6G will enable access to information and services for everyone, fostering economic growth and social inclusion.

APPENDIX B

STEP-BY-STEP SIMULATION IN CST

This appendix provides a detailed overview of the steps followed in CST Studio Suite to design and simulate the RIS project. The process is divided into several stages: project creation, unit cell design, simulation setup for the unit cell, and full array simulation. Below is a step-by-step description of the workflow.

B.1. Project Creation

The design process begins by creating a new project using the appropriate CST template:

1. Open CST Studio and select `Project -> New Template`.
2. Navigate to `Microwaves & RF/OPTICAL` and choose the `Periodic Structure` template (as shown in Figure B.1).
3. Select the template for `FSS, Metamaterial - Unit Cell`.
4. Choose a workflow by selecting `Phase Diagram` in the Frequency Domain.
5. Set the default units (e.g., mm, GHz) and define the minimum and maximum frequency values as shown in Figure B.2.

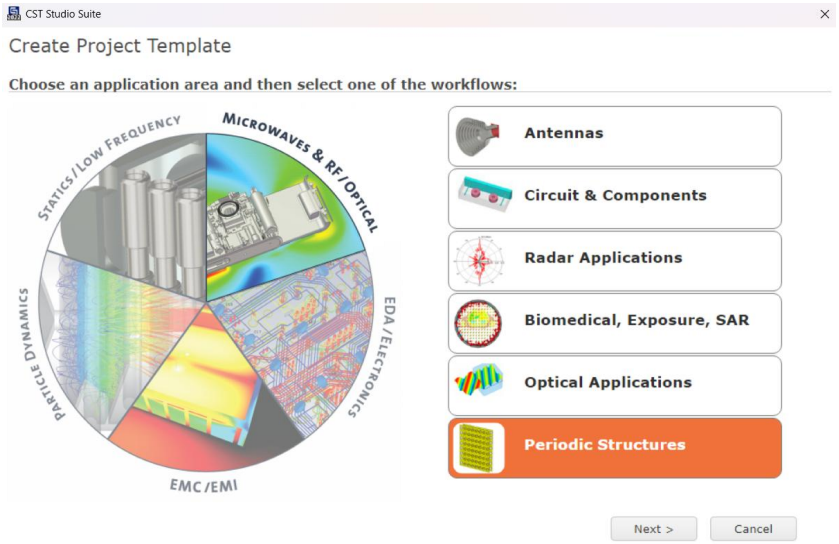

Figure B.1.: CST Studio project template selection for a periodic structure.

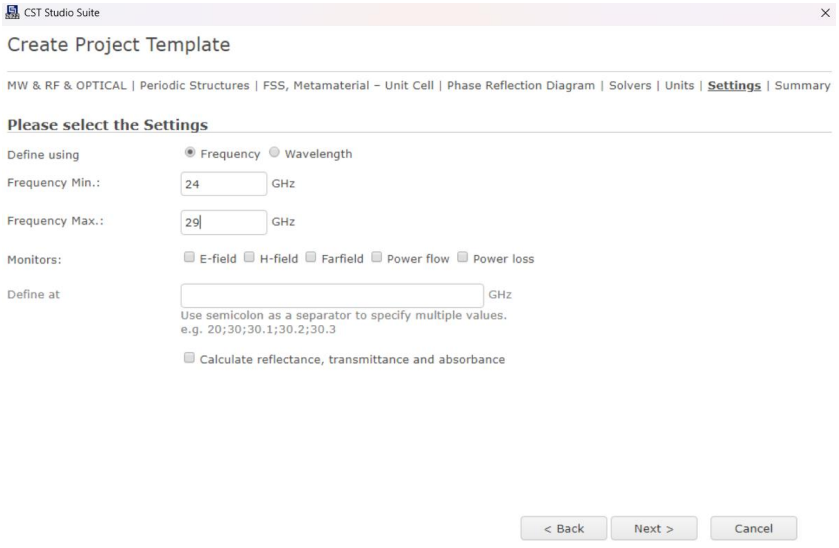

Figure B.2.: CST Studio project template selection for a periodic structure.

B.2. Unit Cell Design

The unit cell is designed using CST's modeling tools:

1. Access the `Material Library` via `Modeling -> Material Library -> Load From Library` and select FR-4 for the substrate (see Figure B.3) and copper for the conductive elements (see Figure B.4).

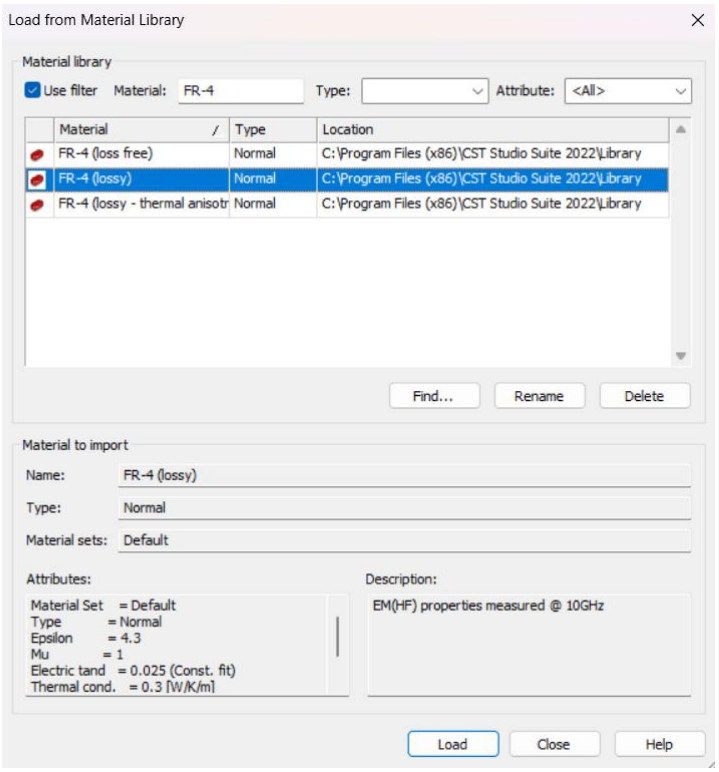

Figure B.3.: Selection of FR-4 material in CST's Material Library.

2. Define geometric primitives (bricks, shapes) and assign adequate materials to the faces and edges. Utilize Boolean operations, bending tools, and other modeling features as necessary to achieve the final unit cell design, as shown in Figure B.5.

B.3. Simulation Setup for the Unit Cell

Once the unit cell is modeled, the simulation is configured as follows:

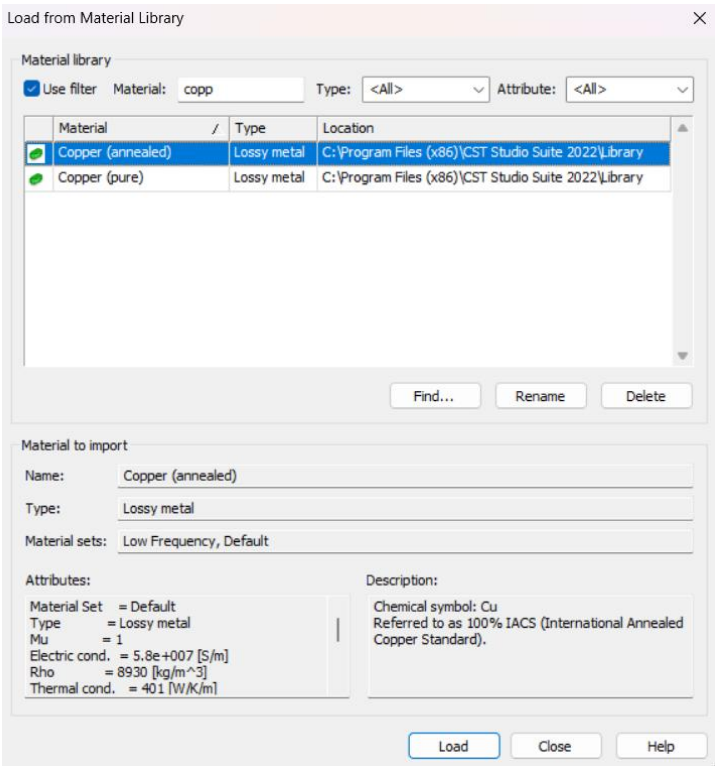

Figure B.4.: Selection of copper material in CST's Material Library.

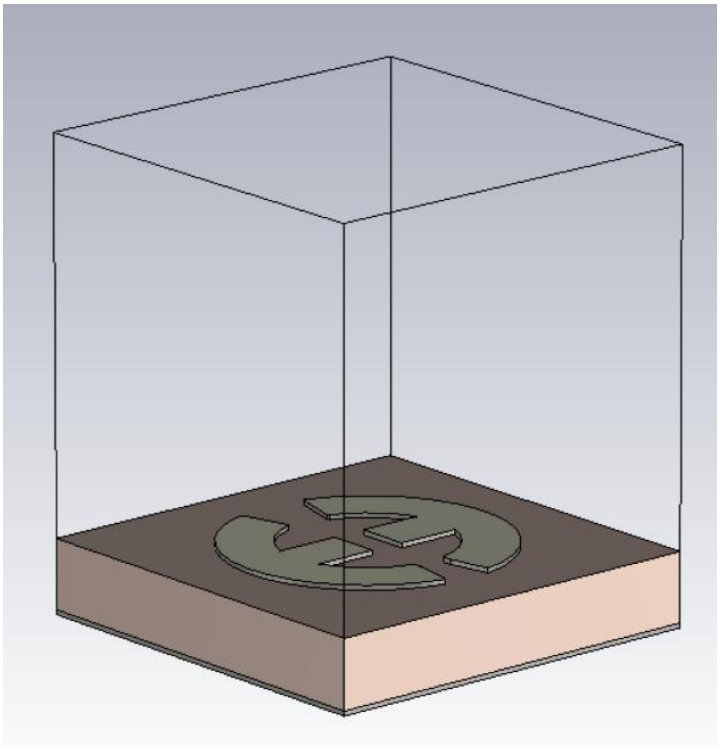

Figure B.5.: Final design of the unit cell using geometric primitives and Boolean operations.

1. Go to `Simulation -> Lumped Element` and select the relevant edges to choose the position of the varactor and then create variables for varactor values (see Figure B.6).

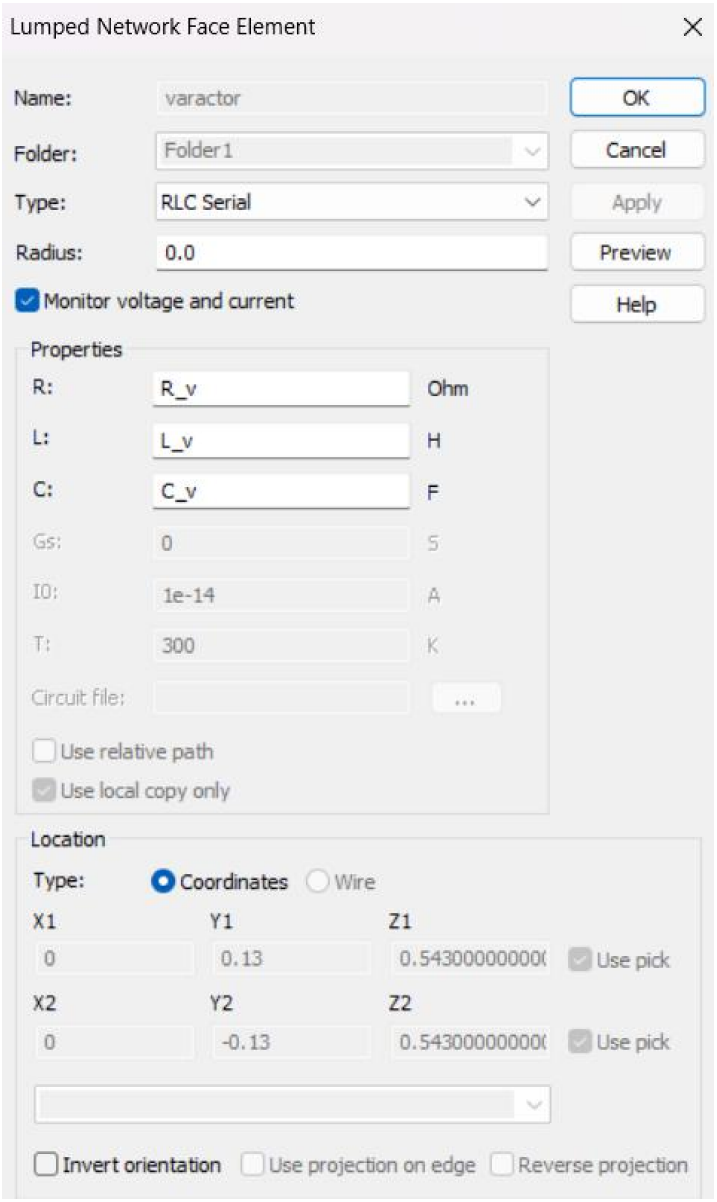

Figure B.6.: Implementation of the Varactor as a Lumped Element in CST

2. Configure the port settings by accessing `Port -> Settings for Floquet Boundaries` and graphically setting the distance to the reference plane, as shown in Figure B.7.

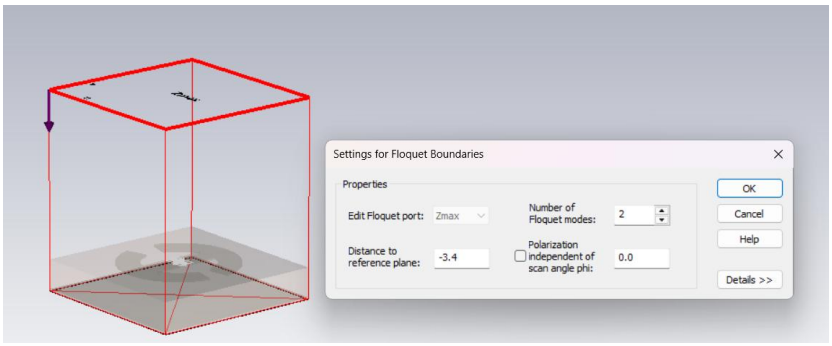

Figure B.7.: Configuration of Floquet Boundary Settings and Distance to Reference Plane in CST.

3. Set up a parameter sweep for the capacitance values of the varactor via `Simulation -> Parameter Sweep`, as illustrated in Figure B.8.

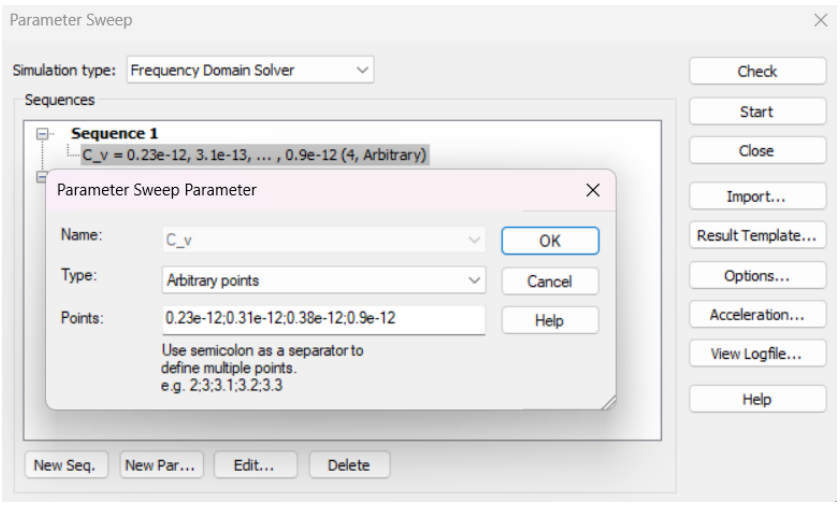

Figure B.8.: Parameter Sweep Setup for Capacitance Values in CST.

B.4. Unit Cell Results

The simulation results for the unit cell are obtained by:

1. Analyzing the 1D results under `S11` to view the amplitude (linear or in dB) and phase response, as shown in Figure B.9.

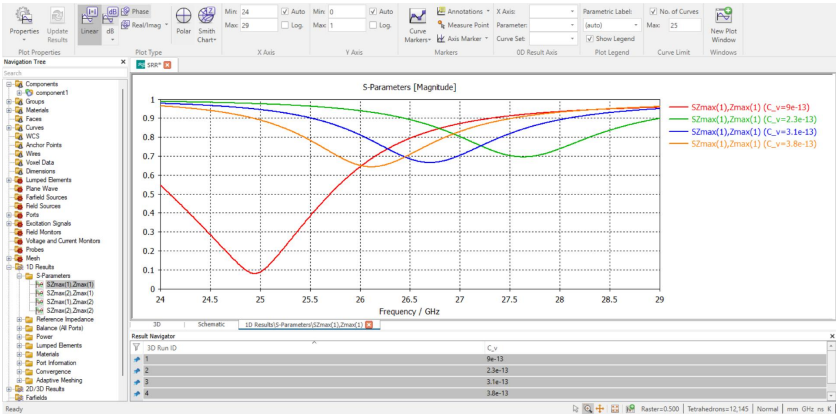

Figure B.9.: S11 Results Showing Linear Amplitude and Phase Response.

B.5. Array Simulation

After validating the unit cell, the full RIS array is simulated following these steps:

1. Start a new simulation project by navigating to `Home -> Simulation Project -> Array Task -> Array Properties` (as shown in Figure B.10) and create the full array simulation project.

2. Set up the excitation by selecting `Simulation -> Plane Wave -> Plane Wave Settings`. Configure the propagation vector according to the desired incidence angles (as described in Chapter 4) and ensure the distance to the decoupling plane matches the Floquet Port's reference plane, as illustrated in Figure B.11.

3. Use the VBA Macro Editor by selecting `Macro -> Open VBA Macro Editor`. Open and run the required files containing the five macros detailed in Appendix C (one for applying the varactor settings for each encoding and one for assembling the unit cells into the full array), as shown in Figure B.12.

4. Configure the field monitor by accessing `Simulation -> Field Monitor` and selecting the RCS/Far Field Monitor settings, choosing the appropriate frequency of operation, as shown in Figure B.13.

5. In the Time Domain Solver, adjust the accuracy, mesh type, and source wave settings. Mesh refinement is disabled due to the large problem size, as illustrated in Figure B.14.

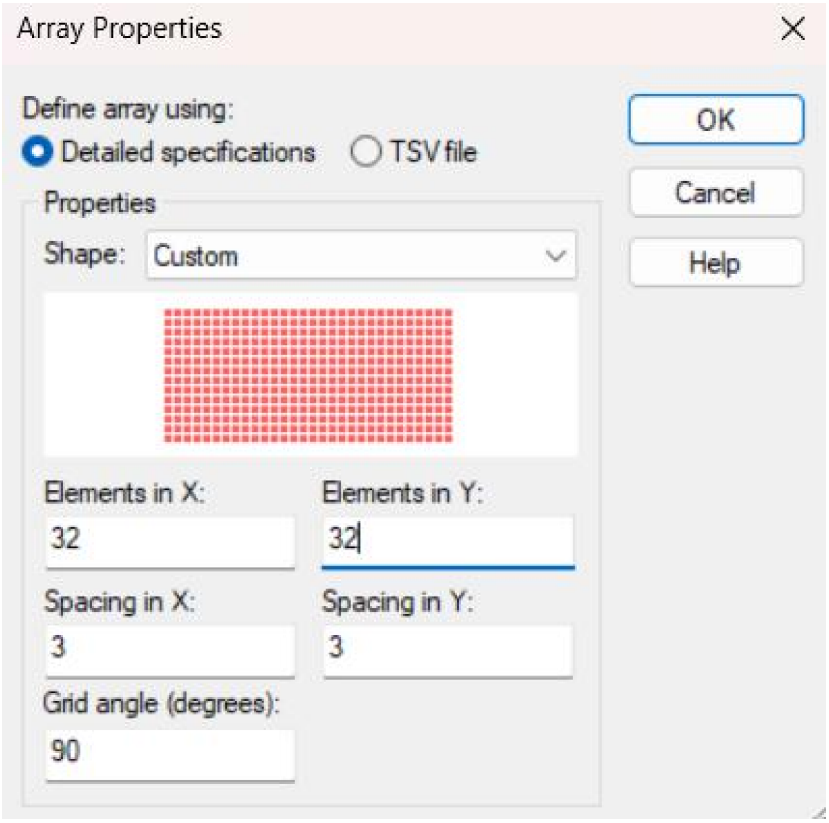

Figure B.10.: Array Properties Setup for Full Array Simulation in CST.

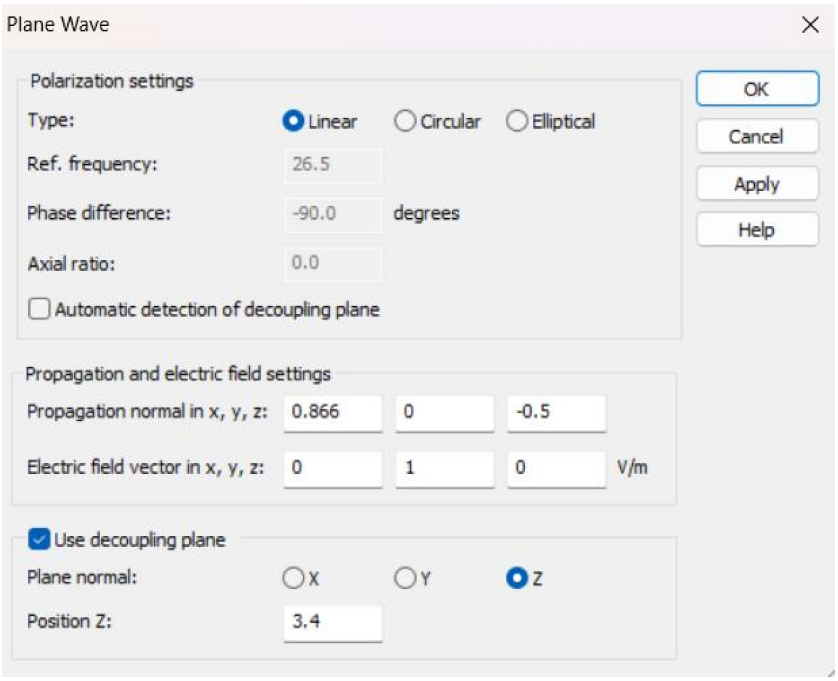

Figure B.11.: Plane Wave Settings for Excitation in CST.

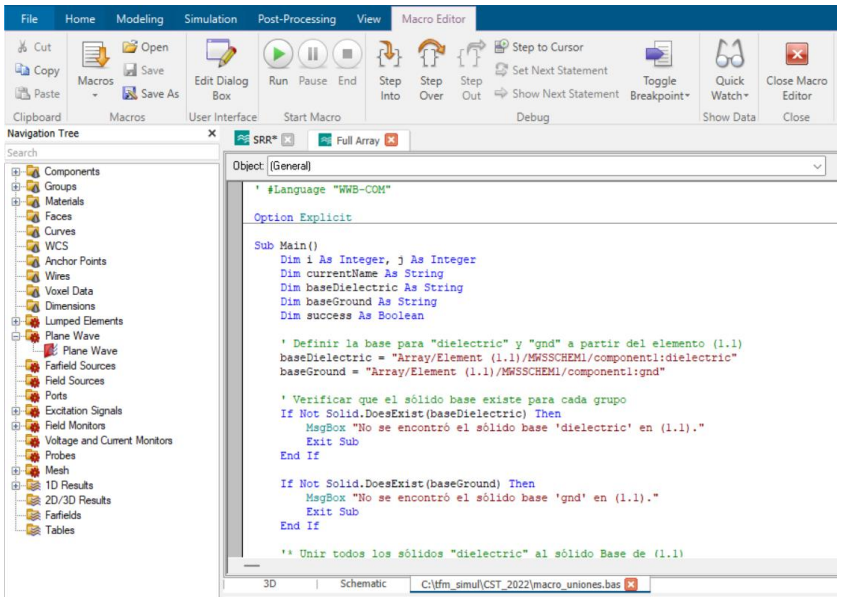

Figure B.12.: VBA Macro Editor Interface in CST.

B.6. Array Results

The final simulation results for the RIS array are presented in 1D, 2D, and 3D RCS plots (in linear scale or expressed in dB), as shown in Chapter 4.

This detailed workflow in CST Studio has enabled the design, simulation, and analysis of both the unit cell and the full RIS array, providing valuable insights into its performance for beam steering applications.

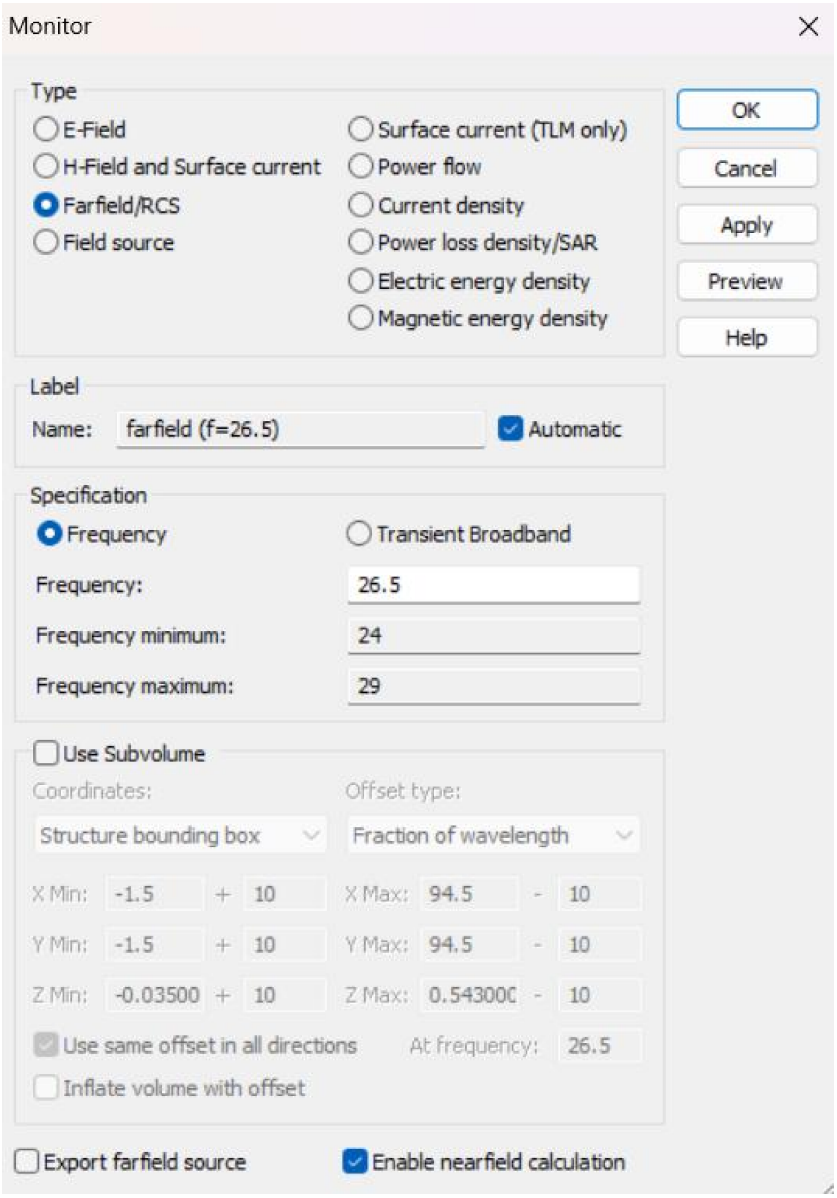

Figure B.13.: Field Monitor Settings for RCS and Far Field Analysis.

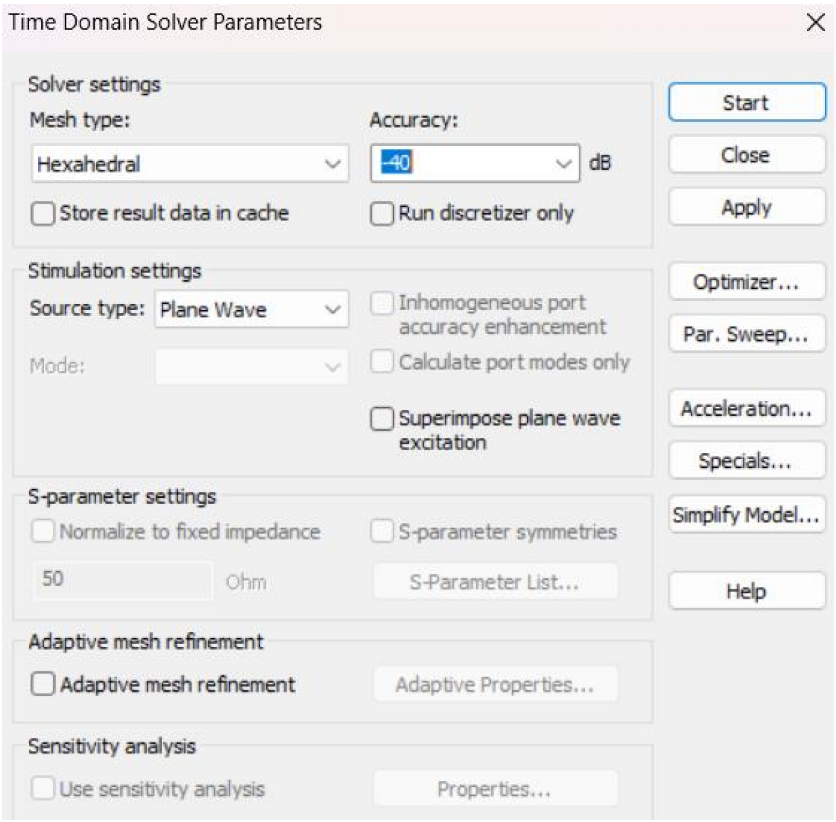

Figure B.14.: Time Domain Solver Settings in CST.

APPENDIX C

VBA Macros for CST

This appendix presents the VBA macros developed to facilitate the CST simulations. A total of five scripts have been implemented. The first macro merges all the dielectric material and the lower ground plane of the unit cells, thereby reducing the computational load. The following macros implement a linear coding strategy for the RIS array, with configurations ranging from $N = 1$ to $N = 4$.

C.1. Macro 1: Merging Dielectric and Lower Ground Plane

This macro applies unions between the ground layers and between the dielectric layers of the different unit cells within the RIS array. Specifically, it merges all dielectric solids with the base dielectric in the reference element located at position (1,1) and does the same for the ground solids. This approach reduces the number of separate objects in the CST model, leading to a lower computational load and faster simulation times. By unifying these layers, the complexity of the electromagnetic interactions is also simplified, maintaining the physical accuracy needed for the simulations.

```
1  ' VBA Macro: Merge Dielectric and Lower Ground Plane
2  ' This macro merges all dielectric solids with the base dielectric in (1,1)
3  ' and all ground solids with the base ground in (1,1) to reduce computational load.

4  Option Explicit

5  Sub Main()
6      Dim i As Integer, j As Integer
```

```
    Dim currentName As String
    Dim baseDielectric As String
    Dim baseGround As String
    Dim success As Boolean

    ' Define the base for "dielectric" and "gnd" from the element (1,1)
    baseDielectric = "Array/Element (1.1)/MWSSCHEM1/component1:dielectric"
    baseGround = "Array/Element (1.1)/MWSSCHEM1/component1:gnd"

    ' Check if the base solids exist
    If Not Solid.DoesExist(baseDielectric) Then
        MsgBox "Base 'dielectric' solid not found in (1,1)."
        Exit Sub
    End If

    If Not Solid.DoesExist(baseGround) Then
        MsgBox "Base 'gnd' solid not found in (1,1)."
        Exit Sub
    End If

    ' Merge all "dielectric" solids with the base dielectric in (1,1)
    For i = 1 To 36
        For j = 1 To 36
            ' Skip the base element (1,1)
            If Not (i = 1 And j = 1) Then
                currentName = "Array/Element (" & i & "." & j & ")/MWSSCHEM1/component1:dielectric"
                If Solid.DoesExist(currentName) Then
                    success = Solid.AddWithName(currentName, baseDielectric)
                    If success Then
                        Solid.Delete currentName
                    End If
                End If
            End If
        Next j
    Next i

    ' Merge all "gnd" solids with the base ground in (1,1)
    For i = 1 To 36
        For j = 1 To 36
            ' Skip the base element (1,1)
            If Not (i = 1 And j = 1) Then
                currentName = "Array/Element (" & i & "." & j & ")/MWSSCHEM1/component1:gnd"
                If Solid.DoesExist(currentName) Then
                    success = Solid.AddWithName(currentName, baseGround)
                    If success Then
                        Solid.Delete currentName
                    End If
                End If
            End If
        Next j
    Next i

    MsgBox "Dielectric and Ground merging completed successfully."
End Sub
```

Código Fuente C.1.: Macro 1: Merging Dielectric and Lower Ground Plane

C.2. Macro 2: Linear Coding for N=1

This macro applies a linear coding pattern to the RIS array for a configuration where N=1. In this case, each row uses a different capacitance value in a repeating sequence of four.

```
' VBA Macro for Linear Coding N=1
' Each row uses a different capacitance value in a repeating sequence.

Option Explicit
Sub Main()
    Dim elementName As String
    Dim success As Boolean
    Dim resistance As Double, inductance As Double, capacitance As Double
    Dim i As Integer, j As Integer

    ' Define resistance and inductance
    resistance = 1          ' 1 ohm
    inductance = 2e-11      ' 0.02 nH

    ' Define capacitance values for the cyclic pattern
    Dim capacitanceValues(3) As Double
    capacitanceValues(0) = 0.9e-12   ' 0.9 pF
    capacitanceValues(1) = 0.38e-12  ' 0.38 pF
    capacitanceValues(2) = 0.31e-12  ' 0.31 pF
    capacitanceValues(3) = 0.23e-12  ' 0.23 pF

    ' Loop over rows i (1 to 32)
    For i = 1 To 32
        ' Determine capacitance value with N=1
        capacitance = capacitanceValues(((i - 1) \ 1) Mod 4)

        ' Loop over columns j (1 to 32)
        For j = 1 To 32
            ' Construct full element name with path
            elementName = "Array/Element (" & i & "." & j & ")/MWSSCHEM1/Folder1:varactor"

            ' Reset element configuration
            On Error Resume Next
            LumpedElement.Reset
            On Error GoTo 0

            ' Set values before modifying
            On Error Resume Next
            LumpedElement.SetR resistance
            LumpedElement.SetL inductance
            LumpedElement.SetC capacitance
            LumpedElement.SetName elementName
            On Error GoTo 0
```

```
            ' Attempt to modify the element
            success = LumpedElement.Modify
        Next j
    Next i
End Sub
```

Código Fuente C.2.: Macro 2: Linear Coding for N=1

C.3. Macro 3: Linear Coding for N=2

This macro implements the linear coding strategy for the RIS array with a configuration of N=2. In this scheme, each capacitance value is repeated for 2 consecutive rows before moving to the next value.

```
' VBA Macro for Linear Coding N=2
' Each row uses a different capacitance value in a repeating sequence of two.

Option Explicit
Sub Main()
    Dim elementName As String
    Dim success As Boolean
    Dim resistance As Double, inductance As Double, capacitance As Double
    Dim i As Integer, j As Integer

    ' Define resistance and inductance
    resistance = 1          ' 1 ohm
    inductance = 2e-11      ' 0.02 nH

    ' Define capacitance values for the cyclic pattern
    Dim capacitanceValues(3) As Double
    capacitanceValues(0) = 0.9e-12   ' 0.9 pF
    capacitanceValues(1) = 0.38e-12  ' 0.38 pF
    capacitanceValues(2) = 0.31e-12  ' 0.31 pF
    capacitanceValues(3) = 0.23e-12  ' 0.23 pF

    ' Loop over rows i (1 to 32)
    For i = 1 To 32
        ' Determine capacitance value with N=2
        capacitance = capacitanceValues(((i - 1) \ 2) Mod 4)

        ' Loop over columns j (1 to 32)
        For j = 1 To 32
            ' Construct full element name with path
            elementName = "Array/Element (" & i & "." & j & ")/MWSSCHEM1/Folder1:varactor"

            ' Reset element configuration
            On Error Resume Next
            LumpedElement.Reset
            On Error GoTo 0

            ' Set values before modifying
```

```
            On Error Resume Next
            LumpedElement.SetR resistance
            LumpedElement.SetL inductance
            LumpedElement.SetC capacitance
            LumpedElement.SetName elementName
            On Error GoTo 0

            ' Attempt to modify the element
            success = LumpedElement.Modify
        Next j
    Next i
End Sub
```

Código Fuente C.3.: Macro 3: Linear Coding for N=2

C.4. Macro 4: Linear Coding for N=3

This macro applies a linear coding scheme for the RIS array with a configuration of N=3. For N=3, each capacitance value is repeated for 3 rows.

```
' VBA Macro for Linear Coding N=3
' Each row uses a different capacitance value in a repeating sequence of three.

Option Explicit
Sub Main()
    Dim elementName As String
    Dim success As Boolean
    Dim resistance As Double, inductance As Double, capacitance As Double
    Dim i As Integer, j As Integer

    ' Define resistance and inductance
    resistance = 1          ' 1 ohm
    inductance = 2e-11      ' 0.02 nH

    ' Define capacitance values for the cyclic pattern
    Dim capacitanceValues(3) As Double
    capacitanceValues(0) = 0.9e-12   ' 0.9 pF
    capacitanceValues(1) = 0.38e-12  ' 0.38 pF
    capacitanceValues(2) = 0.31e-12  ' 0.31 pF
    capacitanceValues(3) = 0.23e-12  ' 0.23 pF

    ' Loop over rows i (1 to 32)
    For i = 1 To 32
        ' Determine capacitance value with N=3
        capacitance = capacitanceValues(((i - 1) \ 3) Mod 4)

        ' Loop over columns j (1 to 32)
        For j = 1 To 32
            ' Construct full element name with path
            elementName = "Array/Element (" & i & "." & j & ")/MWSSCHEM1/Folder1:varactor"

            ' Reset element configuration
```

```
            On Error Resume Next
            LumpedElement.Reset
            On Error GoTo 0

            ' Set values before modifying
            On Error Resume Next
            LumpedElement.SetR resistance
            LumpedElement.SetL inductance
            LumpedElement.SetC capacitance
            LumpedElement.SetName elementName
            On Error GoTo 0

            ' Attempt to modify the element
            success = LumpedElement.Modify
        Next j
    Next i
End Sub
```

Código Fuente C.4.: Macro 4: Linear Coding for N=3

C.5. Macro 5: Linear Coding for N=4

This macro implements the linear coding approach for the RIS array in the N=4 configuration. This configuration repeats each capacitance value for 4 consecutive rows.

```
' VBA Macro for Linear Coding N=4
' Each row uses a different capacitance value in a repeating sequence of four.

Option Explicit
Sub Main()
    Dim elementName As String
    Dim success As Boolean
    Dim resistance As Double, inductance As Double, capacitance As Double
    Dim i As Integer, j As Integer

    ' Define resistance and inductance
    resistance = 1          ' 1 ohm
    inductance = 2e-11      ' 0.02 nH

    ' Define capacitance values for the cyclic pattern
    Dim capacitanceValues(3) As Double
    capacitanceValues(0) = 0.9e-12   ' 0.9 pF
    capacitanceValues(1) = 0.38e-12  ' 0.38 pF
    capacitanceValues(2) = 0.31e-12  ' 0.31 pF
    capacitanceValues(3) = 0.23e-12  ' 0.23 pF

    ' Loop over rows i (1 to 32)
    For i = 1 To 32
        ' Determine capacitance value with N=4
        capacitance = capacitanceValues(((i - 1) \ 4) Mod 4)
```

```
22          ' Loop over columns j (1 to 32)
23          For j = 1 To 32
24              ' Construct full element name with path
25              elementName = "Array/Element (" & i & "." & j & ")/MWSSCHEM1/Folder1:varactor"

26              ' Reset element configuration
27              On Error Resume Next
28              LumpedElement.Reset
29              On Error GoTo 0

30              ' Set values before modifying
31              On Error Resume Next
32              LumpedElement.SetR resistance
33              LumpedElement.SetL inductance
34              LumpedElement.SetC capacitance
35              LumpedElement.SetName elementName
36              On Error GoTo 0

37              ' Attempt to modify the element
38              success = LumpedElement.Modify
39          Next j
40      Next i
41  End Sub
```

Código Fuente C.5.: Macro 5: Linear Coding for N=4

List of figures

List of Listings

LIST OF TABLES

REFERENCES

[1] Jing Cheng Liang; Qiang Cheng: *An angle-insensitive 3-bit reconfigurable intelligent surface*. https://www.researchgate.net/publication/357156865_An_Angle-Insensitive_3-Bit_Reconfigurable_Intelligent_Surface?enrichId=rgreq-e9de7992fc747ef7f8f64c51ab86a1ff-XXX&enrichSource=Y292ZXJQYWdlOzM1NzE1Njg2NTtBUzoxMTAyMzY2NTg1Njg4MDY0QDE2Mzk4MzYwODMzODc%3D&el=1_x_3&_esc=publicationCoverPdf. Accedido el 24 de Enero de 2025.

[2] Jing Cheng Liang; Qiang Cheng: *On the mobility effect in uav-mounted absorbing metasurfaces: A theoretical and experimental study*. Accedido el 24 de Septiembre de 2024.

[3] Mohammad Abdul; ShukoorSukomal Dey: *A novel modified circular ring-based broadband polarization-insensitive angular stable circuit analog absorber (caa) for rcs applications*. https://www.researchgate.net/publication/359065800_A_novel_modified_circular_ring-based_broadband_polarization-insensitive_angular_stable_circuit_analog_absorber_CAA_for_RCS_applications. Accedido el 20 de Febrero de 2025.

[4] Antonio Clemente; Laurent Dussopt: *Wideband 400-element electronically reconfigurable transmitarray in x band*. https://ieeexplore.ieee.org/document/6547987. Accedido el 11 de Octubre de 2025.

[5] Ericsson: *6g standardization – an overview of timeline and high-level technology principles*. https://www.ericsson.com/en/blog/2024/3/6g-standardization-timeline-and-technology-principles. Accedido el 23 de Octubre de 2024.

[6] Ericsson: *Ericsson mobility report, june 2024*. https://www.ericsson.com/en/reports-and-papers/mobility-report/reports. Accedido el 23 de Octubre de 2024.

[7] Guangyao Liu; Jiaqi Han: *A novel frequency reconfigurable polarization converter based on active metasurface*. https://journals.riverpublishers.com/index.php/ACES/article/download/8347/6859/28397. Accedido el 24 de Octubre de 2025.

[8] Christoph Lipps; Jan Herbst: *A physical layer security perspective*. https://www.researchgate.net/publication/362910842_Reconfigurable_Intelligent_Surfaces_A_Physical_Layer_Security_Perspective/figures?lo=1. Accedido el 24 de Enero de 2025.

[9] Demos Serghiou; Mohsen Khalily: *Terahertz communications for 6g and beyond wireless networks: Challenges, key advancements, and opportunities*. https://www.researchgate.net/publication/362695494_Terahertz_Channel_Propagation_Phenomena_Measurement_Techniques_and_Modeling_for_6G_Wireless_Communication_Applications_a_Survey_Open_Challenges_and_Future_Research_Directions. Accedido el 5 de Noviembre de 2024.

[10] Yuanwei Liu; Xiao Liu: *Reconfigurable intelligent surfaces: Principles and opportunities*. https://www.researchgate.net/publication/342763037_Reconfigurable_Intelligent_Surfaces_Principles_and_Opportunities/link/5f05c507299bf188160a5042/download?_tp=eyJjb250ZXh0Ijp7ImZpcnN0UGFnZSI6InB1YmxpY2F0aW9uIiwicGFnZSI6InB1YmxpY2F0aW9uIn19. Accedido el 20 de Octubre de 2024.

[11] MACOM: *MAVR-000120-14110G Datasheet*. MACOM, 2025. https://www.mouser.es/datasheet/2/249/MAVR_000120_1411-473714.pdf.

[12] Artem R. Vilenskiy; Mikhail N. Makurin: *Reconfigurable transmitarray with near-field coupling to gap waveguide array antenna for efficient 2-d beam steering*. https://ieeexplore.ieee.org/document/9109659. Accedido el 7 de Octubre de 2025.

[13] Marcos Baena Molina; Ángel Palomares-Caballero: *1-bit ris unit cell with mechanical reconfiguration at 28 ghz*. https://ieeexplore.ieee.org/document/10500936/. Accedido el 15 de Enero de 2025.

[14] Jean Baptiste Gros; Vladislav Popov: *A reconfigurable intelligent surface at mmwave based on a binary phase tunable metasurface*. https://ieeexplore.ieee.org/document/9424172. Accedido el 16 de Diciembre de 2024.

[15] Zizhen Zheng; Wu Ren: *A new 1 bit electronically reconfigurable transmitarray*.

https://www.mdpi.com/2079-9292/13/7/1383. Accedido el 11 de Febrero de 2025.

[16] Dassault Systèmes: *CST Studio Suite - User Manual*. Dassault Systèmes, 2023. https://www.3ds.com/products/simulia/cst-studio-suite/.

[17] TMYTEK: *Xrifle dynamic ris*. https://tmytek.com/products/components/xrifle-dynamic-ris#. Accedido el 11 de Octubre de 2024.

[18] Christos Liaskos; Ageliki Tsioliaridou: *Xr-rf imaging enabled by software-defined metasurfaces and machine learning: Foundational vision, technologies and challenges*. https://ieeexplore.ieee.org/document/10196450. Accedido el 21 de Octubre de 2025.

[19] IEEE Communications Surveys Tutorials: *On the road to 6g: Visions, requirements, key technologies and testbeds*. https://www.researchgate.net/publication/368868997_On_the_Road_to_6G_Visions_Requirements_Key_Technologies_and_Testbeds. Accedido el 20 de Octubre de 2024.

[20] Alexandros Pitilakis; Dimitrios Tyrovolas: *On the mobility effect in uav-mounted absorbing metasurfaces: A theoretical and experimental study*. https://ieeexplore.ieee.org/document/10196450. Accedido el 20 de Octubre de 2025.

[21] Linglong Dai; Bichai Wang: *Reconfigurable intelligent surface-based wireless communications: Antenna design, prototyping, and experimental results*. https://ieeexplore.ieee.org/document/9020088. Accedido el 21 de Diciembre de 2024.

[22] Luis Silva; Pei Xiao: *A 2-bit tunable unit cell for 6g reconfigurable intelligent surface application*. https://ieeexplore.ieee.org/document/9769482. Accedido el 3 de Enero de 2025.

[23] Yu Wang; Shenheng Xu: *2 bit reconfigurable unit-cell and electronically steerable transmitarray at ka-band*. https://ieeexplore.ieee.org/document/8920221. Accedido el 15 de Octubre de 2025.

[24] A. H. Abdelrahman; Fan Yang: *Analysis and Design of Transmitarray Antennas*. Springer, 2022, ISBN 9783031015410.

[25] Akram Shafie; Nan Yang: *Terahertz communications for 6g and beyond wireless networks: Challenges, key advancements, and opportunities*. https://arxiv.org/pdf/2207.11021. Accedido el 5 de Noviembre de 2024.

[26] Mohamed Gamal; Abdalrahman Younis: *Varactor diode : A comprehensive overview on all aspects*. https://www.researchgate.net/publication/377691773_Varactor_Diode_A_Comprehensive_Overview_On_All_Aspects. Accedido el 4 de Febrero de 2025.